



### Pilkington Library

Author/Filing Title ..... HAYWOOD .....

Vol. No. .... Class Mark ..... T .....

**Please note that fines are charged on ALL  
overdue items.**

LOAN COPY

0402153308



BADMINTON PRESS  
UNIT 1 BROOK ST  
SYSTON  
LEICESTER, LE7 1GD  
ENGLAND  
TEL : 0116 260 2917  
FAX : 0116 269 6639




Department of Electronic and Electrical Engineering  
Loughborough University of Technology

# An Experimental Synthetic Aperture Sonar

Brett Haywood

A thesis submitted in partial fulfillment of the award of Master of Philosophy at  
Loughborough University of Technology.

August 1998

 Loughborough University Printed Library
Date: Jan 00
Class:
Acc No. 040215330

M0001104LB

## **Abstract**

Aperture synthesis is a mature technique that has been used with success in a number of remote sensing fields. Sonars can also potentially benefit from the technique, though to date the limitations of slow acoustic propagation and difficulty in maintaining a stable platform has hindered investigation.

This thesis investigates aperture synthesis for high resolution underwater imaging. A prototype sonar is designed and fabricated for the study. The performance of the sonar is assessed in both tank and sea trials and the results presented in this thesis.

<b>CHAPTER 1 INTRODUCTION.....</b>	<b>6</b>
1.1 IMAGING SONARS.....	6
1.2 SIDE SCAN SONAR.....	6
1.3 SYNTHETIC APERTURE SIDE SCAN SONAR.....	10
1.4 PURPOSE OF THIS THESIS.....	12
<b>CHAPTER 2 LITERATURE SURVEY.....</b>	<b>15</b>
2.1 INTRODUCTION .....	15
2.2 EARLY RADAR DEVELOPMENTS.....	15
2.3 RECENT SYNTHETIC APERTURE RADAR DEVELOPMENTS .....	18
2.4 SYNTHETIC APERTURE SONAR.....	19
<b>CHAPTER 3 THEORY OF SYNTHETIC APERTURE SONAR .....</b>	<b>27</b>
3.1 INTRODUCTION .....	27
3.2 SYNTHETIC APERTURES .....	28
3.3 SYNTHETIC APERTURE RESOLUTION.....	30
3.4 AMBIGUITIES .....	32
3.4.1 <i>Range Ambiguities</i> .....	32
3.4.2 <i>Azimuth Ambiguities</i> .....	33
3.5 AREA MAPPING.....	34
3.5.1 <i>Multiple Vertical Beams</i> .....	34
3.5.2 <i>Multiple Receive Elements</i> .....	35
3.5.3 <i>Broadband Operation</i> .....	35
3.6 MOTION COMPENSATION .....	35
<b>CHAPTER 4 EXPERIMENTAL SYNTHETIC APERTURE SONAR.....</b>	<b>38</b>
4.1 INTRODUCTION .....	38
4.2 OVERVIEW .....	40
4.3 MOTION MEASUREMENT EQUIPMENT .....	44
4.4 ACOUSTIC SENSORS .....	45
4.5 ACOUSTIC SENSOR ARRAYS.....	49
4.6 ACOUSTIC SENSOR ELECTRONICS.....	52
4.7 SURFACE ELECTRONICS .....	53
4.7.1 <i>VLDS Interface</i> .....	53
4.7.2 <i>Multi-Purpose Interface</i> .....	57
4.8 DATA REPRODUCTION .....	59
4.9 SOFTWARE .....	60
4.9.1 <i>Motion Data Collection Software</i> .....	60
4.9.2 <i>Motion Data Calibration Software</i> .....	60
4.9.3 <i>Acoustic Data Collection Software</i> .....	61
4.9.4 <i>Acoustic Data Transcription Software</i> .....	62
4.9.5 <i>Acoustic Data Calibration Software</i> .....	62
4.9.6 <i>Analysis Software</i> .....	62
<b>CHAPTER 5 RESULTS FROM SYNTHETIC APERTURE SONAR.....</b>	<b>63</b>
5.1 INTRODUCTION .....	63
5.2 SONAR TEST TANK MEASUREMENTS .....	64

5.2.1	<i>Introduction</i> .....	64
5.2.2	<i>Test Tank Experiments</i> .....	65
5.2.3	<i>Test Tank Data</i> .....	67
5.2.4	<i>Simulations</i> .....	69
5.2.5	<i>Real Image Processing</i> .....	70
5.2.6	<i>Synthetic Image Processing</i> .....	71
5.2.7	<i>Conclusions From Test Tank Measurements</i> .....	74
5.3	<b>MOTION MEASUREMENTS</b> .....	75
5.3.1	<i>Introduction</i> .....	75
5.3.2	<i>Motion Experiments</i> .....	75
5.3.3	<i>Motion Data Processing</i> .....	75
5.3.4	<i>Conclusions From Motion Data</i> .....	79
5.4	<b>SONAR MEASUREMENTS</b> .....	80
5.4.1	<i>Introduction</i> .....	80
5.4.2	<i>Experiments</i> .....	80
5.4.3	<i>Processing of Field Data</i> .....	80
5.4.4	<i>Conclusions From Field Experiments</i> .....	82
<b>CHAPTER 6 CONCLUSIONS</b> .....		<b>84</b>
6.1	<b>DISCUSSION</b> .....	<b>84</b>
6.1	<b>FURTHER INVESTIGATION</b> .....	<b>85</b>
<b>REFERENCES</b> .....		<b>86</b>

# **Chapter 1 Introduction**

## **1.1 Imaging Sonars**

This thesis investigates the imaging of the sea floor using a synthetic aperture sonar system. Sea floors are of considerable interest due to the diverse and increasing range of applications with which they are associated. As a consequence of this increasing activity, the need for accurate information on their physical features increases correspondingly. Representations of this information in the form of undersea images from sonar is of interest to a diverse range of people. Marine geologists study the underwater topography for insight into the mineral and oil wealth beneath, fishermen are interested in features that attract marine life, marine engineers are interested in locating areas conducive to the construction underwater structures, while the maritime forces use the information to maintain safe passage.

Side scan sonar systems have been used for a good number of years to image the physical features of the sea floor in both commercial and military applications. Given the impermeability of sea water to electromagnetic radiation, it is the acoustic energy used in sonar that provides a viable means of producing images of large areas in a relatively short period. This type of sonar is active as it produces a short burst of acoustic energy and the images are a representation of the reflected returns. Considerable experience is required in the interpretation of such representations to discern details of topography. Such sonars have attained a level of development where they are generally adequate for producing low resolution images. It is the improvement of such images through synthetic aperture signal processing that is the subject of this work.

## **1.2 Side Scan Sonar**

A side scan sonar consists of a sonar mounted on a tow body that is towed by a cable from a surface vessel. By using a tow body many of the degrading effects of vessel



motion are reduced in the subsequent images. A depiction of such a sonar is shown Fig. 1.1. An acoustic foot print insonifies the sea floor on both sides of the tow body. Pulses of acoustic energy ('pings') are radiated in narrow beams from the platform at regular time intervals to produce the image. This energy travels through the water, being both absorbed and reflected by objects in its path. The change in impedance between the water and sea floor produces a reflection of energy; some of this is received back at the tow body as acoustic echoes. These echoes are detected by hydrophones and amplified in the tow body. They are then transmitted along the cable to the surface vessel. The associated electronic monitoring equipment on the vessel processes them for display on an output device such as a chart recorder. Each received pulse would typically represent a single line on a chart recorder, with subsequent lines being placed beside each other to form an image as the vessel moves across the sea floor. Although a single line conveys little information, the combination of these into a two-dimensional image is of considerable value.

The two-dimensional image produced by such a side scan sonar system is one of acoustic reflectivity over a narrow bandwidth around a fixed operating frequency. It would be desirable if such an image would not vary with equivalent features of the sea floor or with a change in operating frequency. However, in reality this is not possible as differing sea floors have considerably different relative reflectivities for similar physical features. Likewise, for a change in frequency the image can vary considerably. An extreme example of this variation in frequency are specular effects where the acoustic wavelength is of similar dimension to the feature, considerably altering the appearance in the image. Topography is also difficult to interpret without accompanying bathymetry. However, in some cases the topography can be deduced from the image. An example of this would be a shadow region with no acoustic energy 'illumination' where the topographical information can be inferred.

A conventional side scan sonar consists of a linear array of transducers along the body of a tow platform. These are used to create a narrow beam pattern in the azimuth plane and give high resolution in the along track direction. In the across track direction, high resolution is achieved by transmitting an acoustic pulse of short duration. One can think of the resolution cell being of width equal to the beamwidth and length determined by the number of cycles in the acoustic pulse. Improvements to

the resolution along both axes are possible through an increase in the operating frequency (for a fixed array length and number of transmitted cycles). Similarly, an increase in the length of the array can be used to improve the resolution in the along track direction (for a fixed frequency).

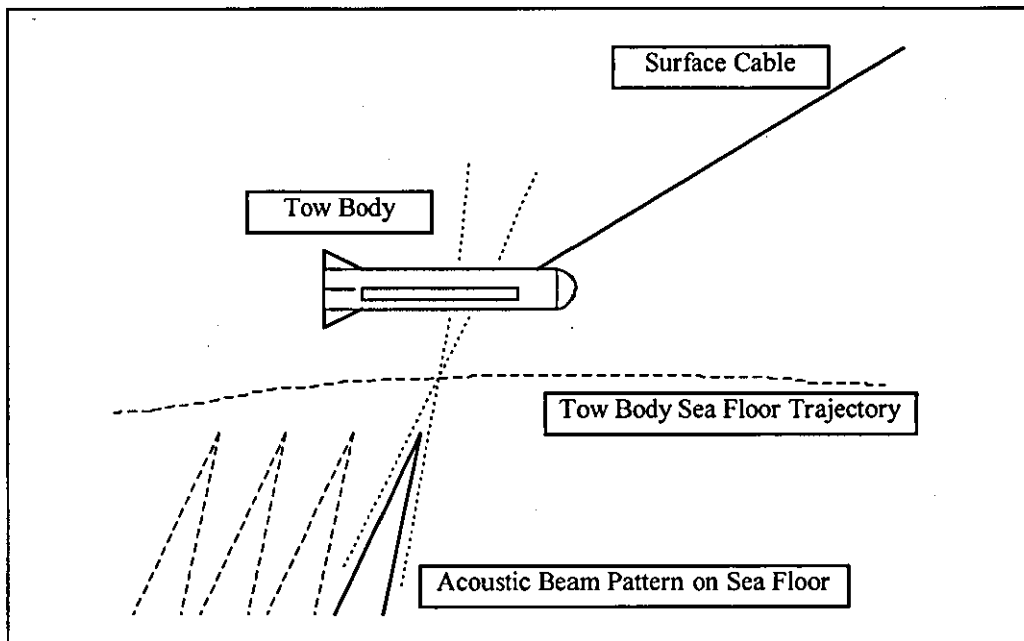


Figure 1.1 Sides can sonar

The along track resolution of a side scan sonar is proportional to the range. Once the near-field distance of the array has been exceeded, the beamwidth increases proportionately with range. As such, the along track resolution increases with distance from the tow body, while the across track resolution remains constant. A consequence of this is that the individual resolution cells become distorted with increasing range. This produces a deterioration in the resolving capability of the sonar.

The signals transmitted from a side scan sonar range in frequency anywhere from 1kHz to 500kHz depending upon the application. The signals are generally narrowband in nature, although a few 'chirped' sonars are now becoming available. There is a compromise between the range and the resolution of a system that must be considered. High frequency transmissions have improved resolving ability, but due to water absorption of the signals they suffer a restriction in range of operation. At low frequencies the range of operation improves, though at the expense of resolution. Another constraint that often necessitates the use of higher frequencies is the physical

length of the array to produce a sufficiently narrow azimuth resolution. Lower frequencies require longer arrays for a given beamwidth. As the array length increases the tow body increases in dimension, becoming heavier and more difficult to deploy, whilst also potentially requiring a larger tow vessel.

A number of side scan sonars have been developed and an historical account was published in a tutorial paper by M. Somers and A. Stubbs (Somers and Stubbs, 1984). Perhaps the most famous is that of GLORIA (Geological Long Range Inclined Asdic). This sonar was designed for continental shelf science and uses a frequency (36kHz) to ensure a good range capability. It has the capability to map an area of 750 km/hr with an azimuth beamwidth of 2.7 degrees and range resolution of 22m. Details of this can be found in a paper by A. Laughton (Laughton, 1981). In contrast to GLORIA, both in dimension and resolving power, are the high resolution side scans. One such device is produced by Klein Associates Inc. This product has an operating frequency of 500kHz and is restricted in range to only 100m. It has an azimuth beamwidth of 0.2 degrees and range resolution of 0.03m.

Commercial side scan sonars have not advanced greatly since the late 1960's. Improvements in electronics and computing have replaced the original analogue processing with the digital equivalent. Chart recorders have also been replaced with video display systems. These have improved the output of the systems considerably, but the principles of operation remain the same. Perhaps the most innovative development to appear recently is the focussed, multiple beam, side scan sonar; one such sonar is also produced by Klein Associates Inc. A prototype of a similar system was demonstrated by P. Fox (Fox, 1985) as a doctoral dissertation. Here five independent azimuth beams are formed simultaneously from each acoustic transmission, giving the tow fish a proportionate increase in tow speed. In addition to this, each resolution cell has compensation for the phase distortion associated with the near-field, improving the resolution of the image considerably.

### 1.3 Synthetic Aperture Side Scan Sonar

The synthetic aperture sonar (SAS) considered in this study operates in a similar manner to a side scan sonar. The sonar is towed behind a surface vessel in an underwater tow body. In contrast to the conventional side scan, the resolution of the sonar image can be processed to prevent degradation with increasing range. The individual resolution cells do not distort in the along track direction, regardless of the distance from the tow body. The SAS represents the next significant development of side scan sonars. To date the technical difficulties of developing such a system have hindered it, though as real-time processing power advances many of these will shortly be overcome.

The principle of operation of a synthetic aperture sonar is based upon the observation that the performance of a real array containing equally spaced elements can be achieved by a single element. This element is moved sequentially across the spatial positions of an array and at each both the amplitude and phase of the echoes from acoustic transmissions are stored. After traversing the array length, the stored data is processed in a manner to synthesise an array aperture, known as a synthetic aperture. There remains an upper limit to the size of this synthetic aperture, this being the distance over which a target remains within the beam pattern of the individual element.

The operation of a synthetic side scan sonar is similar to that of a conventional side scan. The similarity with a side scan sonar is shown in Fig. 1.2. Note that the depicted acoustic foot print is narrower than the conventional side scan case. Repeated pulses of acoustic energy are transmitted from the towfish and these are received by one or more acoustic elements. The significant difference is that the transmitted pulses have a broad azimuth beam width. It is only after the aperture is traversed that a narrow beam is produced from the stored data. The synthetic side scan image does not appear as each echo is received, rather there is a time delay until the entire length of the synthetic aperture has been traversed and the beam computed before the line on the display appears.

The simplest synthetic aperture processing is that of the unfocussed aperture. No account is made for any geometric phase distortions at subsequent positions along the synthetic aperture. As there are no phase adjustments to the received waveforms there is a limit to the length of the aperture that can be synthesised (in addition to the element beamwidth restriction) through geometric coherence limits. This limit occurs at a given range when the round-trip distance from a target to the centre of the synthetic array differs by one-quarter wavelength from the round-trip distance from the target and the extremities of the synthetic array. Once this limit is exceeded destructive interference occurs and the image quality degrades.

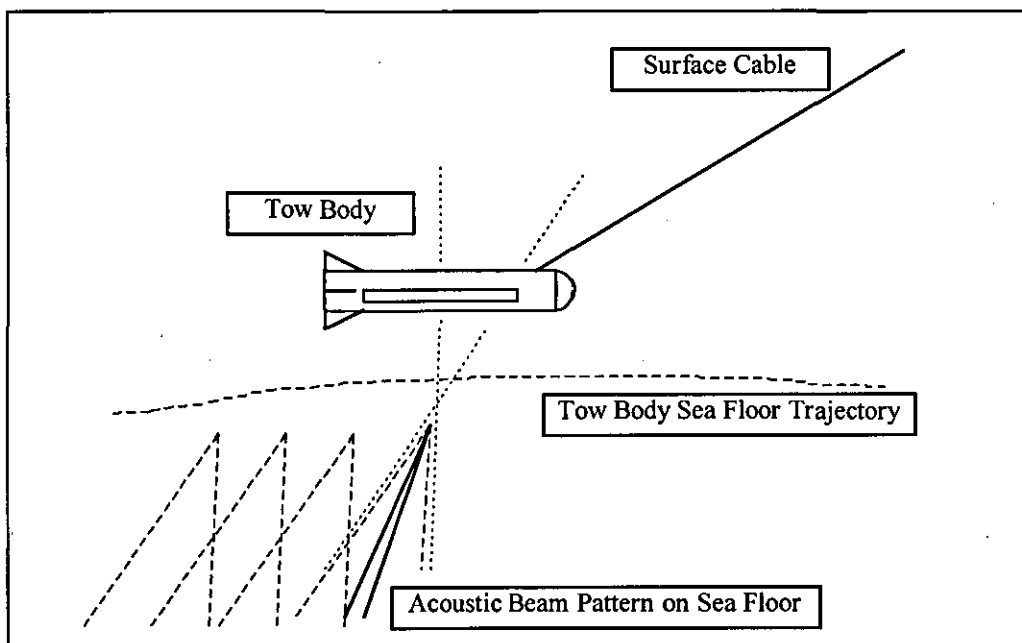


**Figure 1.2 Synthetic Aperture Sonar**

Elaborate synthetic aperture processing systems involve adjusting the phases of the received waveforms so that geometric distortion does not degrade the image. This produces a focussed image. Here the waveforms are combined coherently after adjustments for phase differences are made. This removes the coherence limitation to the synthetic array length so that the element beamwidth constraint dominates. With such processing the resolution cell width can be processed to remain of constant size at all ranges. This is done by changing the synthetic aperture length for all ranges, such that the full aperture length is only used at the most distant range. Closer ranges process a subset of this full synthetic aperture length to keep the resolution cell of constant width.

The performance improvements of synthetic aperture processing do come at a cost over conventional processing. The synthetic aperture must be spatially sampled twice as frequently as a real array to avoid azimuth ambiguities in the image. Synthetic processing is also significantly more computationally intensive as acoustic data must be stored in memory until the entire synthetic aperture has been traversed and image processing completed. The real-time production of images with such processing is still a challenging exercise with existing technologies.

This discussion has assumed that the acoustic propagation medium is constant in time and each subsequent echo return will not fluctuate in phase due to variations in the medium. It also assumes that the path of the individual element in forming the synthetic aperture accurately follows a known path. Unfortunately, a real implementation of a synthetic aperture sonar may not necessarily be able to assume these. These two significant limiting factors have also impeded the production of such a system to date. Prototype systems have been deployed, though most of these used fixed rails with ropes and pulleys to remove unwanted platform motions. Only in a few instances have the prototypes resembled the towbody arrangement that might be expected for an actual production system.

#### **1.4 Purpose of this Thesis**

The aim of this thesis is to demonstrate the development of a synthetic aperture sonar capable of high resolution imaging of the sea floor. This sonar includes three key features that would potentially overcome inherent limitations in developing a practical system. This is the first time that all have been designed into an unconstrained synthetic sonar system. The first feature is a motion measuring system to monitor deviations from the ideal track. The second feature is the presence of multiple receive elements to improve tow speed without degradation through azimuth ambiguities. The third feature is frequency diversity in the acoustic transmissions to reduce the incidence of specular returns and render more representative images of the sea floor.

The inertial motion measurements made on the tow body are not intended to be definitive. The transducers do not have sufficient sensitivity to track the body to sub-wavelength accuracy. As such, the measured motions are only intended to track large deviations that are not low in frequency. These measurements are intended to act as a first order correction to the phase of the received echoes. Once combined with the acoustic measurements further signal and image processing techniques are intended to improve the tracking of the body through space. This additional processing would also remove motion effects that cannot be measured with inertial instruments, such as the additional constant motion offsets produced by currents in the sea.

The use of multiple receivers on the synthetic aperture sonar is intended to allow an increase in the tow velocity without causing azimuth ambiguities. As the synthetic aperture must be spatially sampled twice as frequently as a real array, their use allows an improvement in tow speed. With multiple receive elements the vernier processing technique can be used and the tow speed increased proportionately to the number of elements.

*explains*

The frequency diversity associated with the acoustic transmissions has implications for the image formation. A conventional sonar is narrowband at a single centre frequency. As such, the image produced is one of the backscatter strength at only this frequency. The technique here combines a number of narrowband frequencies, such that the resulting image is an average across an ensemble of available frequencies. An incoherent combination of these images reduces the specular nature of highly coherent imaging, producing a more representative description of the sea floor.

The application of synthetic aperture processing to imaging of the sea floor has received considerable interest of late. The current state of development is discussed in Chapter 2 with a literature survey of the research area. Included in this are the developments in synthetic aperture radar that have had a significant influence on both the early emergence of synthetic processing and the application of the processing techniques presented in this thesis.

The theory of synthetic aperture processing is presented in Chapter 3. The presentation identifies constraints imposed on an operational sonar system and discusses techniques that reduce the impact of these constraints.

A detailed description of the design of the experimental synthetic aperture sonar is presented in Chapter 4. This design is original and embraces a range of disciplines including; transducer design, antenna array design, electronic instrumentation and real time software. The discussion has considerable detail as most of the components in the design are original.

Results of experimentation in both a controlled test tank and in the open sea are discussed in Chapter 5. In support of these results are simulations intended to demonstrate predicted performance of the sonar in ideal conditions.

Conclusions that can be drawn from this research effort are given in Chapter 6.

This thesis is original except for the background theory in the early chapters.



## **Chapter 2 Literature Survey**

### **2.1 Introduction**

Much of the theory applied to synthetic aperture sonar was originally developed in the context of synthetic aperture radar (SAR). There has been considerable effort devoted to radar processing and synthetic array applications are quite common in the field. This chapter traces the early developments in radar processing and follows these into more recent years. The discussion of the more recent developments concentrates on those publications that have a direct implication for synthetic aperture sonar, in particular, the motion compensation aspects. It then focuses on the emergence of synthetic aperture sonar and demonstrates how the field has developed over the last few decades.

### **2.2 Early Radar Developments**

It is not surprising that most of the developments in synthetic array processing came from military applications. Radar emerged early this century as a method of detecting and tracking ships, with the first such system demonstrated by the German Christian Hulsmeyer in 1903. Airborne radar systems for the detection and tracking of aircraft were also being developed at that time, with one particularly active group being at the Naval Research Laboratory in the USA. It was not until 1934 that A. H. Taylor produced an example of such a system from this laboratory. Great Britain and Germany were also developing airborne radars and they demonstrated a capability to produce such systems by 1935. Radar technology spread outside these countries and by the time of World War 2 all the major world powers had an aircraft tracking capability.

In the early 1950's it was realised there was an alternative to rotating an antenna to scan a target area. Sensors fixed to the fuselage of an aircraft could project a beam perpendicular to the direction of travel, this being a side looking radar. As the aircraft

flew across the landscape swathes of the ground could be imaged at a relatively high speed. This technique resulted in an improved along track resolution due to the increased aperture length over a ground based radar. Such systems were built at the time and used for military reconnaissance purposes. These systems used conventional array processing in the production of ground images, but were still able to achieve resolutions in the range of 10-20m due to their high centre frequencies of transmission.

It is generally accepted that Carl Wiley of the Goodyear Aircraft Corporation made the first references to synthetic aperture radar processing in June, 1951 (Wiley, 1985). He referred to his technique as Doppler beam sharpening in the patent application (Wiley, 1965). Wiley observed that the reflections from two fixed targets at an angular separation could be resolved by frequency analysis of the along track spectrum. This permits the azimuth resolution of the return echoes to be enhanced by separating the echoes into groups based on Doppler shift. The concept was pursued by Goodyear and the first airborne synthetic aperture radar flew in 1953.

Independent of the work by Wiley was the research being carried out on moving target detection at the University of Illinois under C. W. Sherwin. This was also based on Doppler characteristics. A member of the group, John Kovaly, noted that variations in terrain height produced distinctive peaks that migrated across the azimuth frequency spectrum. They made experimental observations and formed concepts that provided the basis for a new radar with improved angular resolution. Sherwin first reported the concept of a fully focused array by applying the appropriate phase correction at each range. The phase correction being such that the resulting phases resembled those that would have been obtained by an aircraft flying in a circle with the target at its centre. These developments were all classified and it was not until 1962 that Sherwin published a tutorial paper in the open literature (Sherwin, 1962) on their earlier work.

Following on from the Illinois group a much larger effort was instigated at the University of Michigan, under the name Project Wolverine. The US Army was their sponsor and the goal was to develop a high performance combat surveillance radar. The results of the effort were published by L. J. Cutrona in 1961 (Cutrona, 1961) with

detailed strip maps of Detroit and Washington produced by synthetic aperture techniques.

A discussion paper by Cutrona the following year (Cutrona and Hall, 1962) examined three techniques for obtaining fine azimuth resolution. These were a conventional linear array, an unfocused synthetic aperture and a focused synthetic aperture; with an evaluation of the merits of each. The discussion showed that the resolution of a conventional array could be improved by either increasing the array length or by using a higher centre frequency. With the unfocused synthetic aperture the resolution is not dependent upon array length, but could be improved with a higher centre frequency. In this case there is a maximum length to the synthetic aperture that can be created, a consequence of increasing geometric phase distortions as the synthetic array increases in length. In contrast, the resolution of a focused synthetic aperture is found to be constant and independent of operating frequency. Here the resolution improves as the real aperture length decreases, this being a directly opposite result to the case of the conventional array. As the length of the real aperture decreases the associated beamwidth increases and the length of the synthetic aperture can be increased with this wider illuminated area.

Another paper published at the same time by R. C. Heimiller (Heimiller, 1962) discusses further principles of synthetic arrays. He examines the gain patterns of both focused and unfocused synthetic apertures and notes the effects of different weighting functions in the beamforming. He also discussed the possible sources of phase errors and tabulated the consequences of these. He asserted that the propagation medium and vehicle motion are the two major sources of phase error. The consequences of these phase error sources include:

1. Increased sidelobe level.
2. Beam pointing error.
3. Gain reduction.
4. Beam spreading.
5. Beam wander.

## 2.3 Recent Synthetic Aperture Radar Developments

The level of research in synthetic aperture radar has been considerable in recent years. These radars include those that are aircraft mounted and those that are satellite borne. Most publications on the topic are not of direct relevance to synthetic aperture sonar and are not discussed here. However, the papers dealing with motion compensation are of considerable interest. A small selection of such papers is presented.

To produce high quality SAR imagery it was recognised early in development that compensation for across track motion was necessary. Methods for this were developed, such as those by J. C. Kirk (Kirk, 1975). He developed a consistent motion compensation approach for all types of SAR imagery, strip mapping, spotlight mapping and Doppler beam sharpened mapping. The technique relied upon measurements from inertial navigation sensors to correct the phase of the measured data. The measurements were used by the signal processor in the synthetic image formation.

Efforts have been made to overcome the reliance on inertial navigation measurements. Such measurements may not be available or their quality maybe poor. Discussions of alternative techniques using autofocus are numerous. One more recent paper was by D. Blacknell and S. Quegan (Blacknell and Quegan, 1991). They examine the contrast optimization autofocus algorithm and note strong evidence to support it being equivalent to minimizing the mean square error between the SAR platform trajectory and a quadratic trajectory over the aperture. This technique is applied iteratively and strives to maximise the contrast across the image. An earlier paper that details the technique is that by J. Wood (Wood, 1988).

Alternative techniques for motion correction are available, with a more promising example being the phase gradient autofocus algorithm. This is discussed in a paper by D. Ghiglia and G. Mastin (Ghiglia and Mastin, 1989) and a later one by D. Wahl et al (Wahl, 1994). This technique is applied iteratively in estimating the phase deviation from the degraded point spread function at a convenient image point. The image is reconstructed with adjusted phase values and then the phase deviation is recalculated.

This process is repeated until the phase errors become acceptably low. The iterative nature of this technique makes it computationally expensive and less suitable to real time implementations.

## 2.4 Synthetic Aperture Sonar

Synthetic aperture processing in the ocean can be either active or passive in nature. For a passive implementation the received acoustic energy is not generated by the system itself, but is radiated from surrounding objects. As only low frequency acoustic energy will propagate a reasonable distance these sonars generally do not have imaging applications. Interest has increased recently in passive synthetic apertures, although the field is not as developed as that for sea floor imaging. The passive synthetic aperture is sufficiently removed from the imaging application that it has not been discussed at length here.

Activity in synthetic aperture processing techniques for underwater imaging first appeared in the late 1960's. A feasibility study was submitted to the U.S. Oceanographic Office by the Raytheon Company (Walsh, 1967) for the design of a high resolution mapping tool. There is no record of this being pursued at the time.

Other preliminary work was performed by a team at John Hopkins University (Bucknam et al., 1971). They described a design for a synthetic aperture sonar and contrasted the likely performance to a conventional side scan sonar.

A short paper by Winston Kock (Kock, 1972) addressed the aperture sampling constraints in synthetic aperture sonar. He discusses a technique that employs multiple receivers for the collection of acoustic data to relax these sampling constraints. Each receiver is placed a fixed distance apart in an array and they all collect data from the acoustic transmissions. An example examines a towed array application (passive sonar) where the restriction imposed on tow speed by the use of a single receive sensor is highlighted. The use of multiple receivers is the suggested technique to increase the tow speed to a practical level.

Perhaps the first paper to appear in the more general acoustics press was that by T. Sato, M. Ueda and S. Fukuda (Sato et al, 1973). They described a laboratory test system that successfully produced a synthetic aperture image at ultrasonic frequencies. They imaged a strand of steel wire and demonstrated the improved resolving ability over conventional beamforming techniques. Work with this group at the Tokyo Institute of Technology continued into the 1980's, with their efforts concentrating upon theoretical studies and laboratory test jigs for verification (Sato and Ikeda, 1977, Ikeda et al, 1979, Ikeda and Sato, 1980, Ikeda et al, 1985). At no time did they attempt to move their test systems beyond the controlled environment of the laboratory.

One of the early workers in synthetic aperture radar, L. J. Cutrona, moved into the field of underwater acoustics when he transferred to the Scripps Institute of Oceanography, University of California. He produced two papers, one in 1975 and the other in 1977, that placed the comparison between synthetic aperture sonars and conventional sonars on a sound theoretical base (Cutrona, 1975, Cutrona, 1977). He describes design procedures to allow an unambiguous range for a desired resolution. In particular, one of the more important results is the demonstration that by radiating multiple beams one can avoid situations in which some combinations of unambiguous range and along track resolution are not achievable.

An ambitious synthetic aperture experiment was described by R. Williams (Williams, 1976) of Columbia University. This was supported by the Naval Research Laboratory, U.S.A, and although not an imaging application it indicates the considerable interest in synthetic aperture techniques at the time. This experiment was aimed at testing the feasibility of replacing towed arrays with a single receiver and creating an aperture with synthetic techniques. They indirectly did this by towing a transmitter and receiving the signals on a moored, two element array. Despite significant difficulties in processing the subsequent data, they were able to synthesise apertures in excess of 1000m at frequencies below 1kHz. The temporal coherence times associated with forming these apertures were of duration greater than several minutes. This was all concluded without having precise navigation for the towed transmitter.

Many of the early contributions to synthetic aperture sonar were comparisons with the radar equivalent. One particular paper by H. Lee (Lee, 1979) observes that it is the slow sound propagation speed in water, as opposed to that in radar, that poses a significant problem in producing a synthetic aperture sonar with satisfactory mapping rates. He suggests the use of multiple receivers to increase the rate, with the increase being proportional to the number of transducers utilised. He also suggests the investigation of the use of motion compensation techniques as those used in synthetic aperture radar.

It was recognised from the outset that both transducer motion and the phase stability of the ocean medium were the two most significant potential sources of degradation in synthetic aperture sonar performance. An experiment was performed in the early 1980's to assess the temporal phase stability of the ocean medium at 100kHz, a potential operating frequency of such an imaging sonar. This experiment is discussed in a paper by J. Christoff, C. Loggins and E. Pipkin (Christoff et al., 1982) from measurements that were made over a two year period. They found that for a propagation distance of 50m., phase coherency of 0.04 radians over a 20 minute period was possible at water depths greater than 75% of the total depth. In shallower depths than this the phase errors increased significantly to 0.31 radians over a 2 minute period. They concluded that, provided a minimum depth was met, the degrading effects of temporal coherence would not have a significant influence upon the formation of a synthetic aperture.

The practical difficulties in producing a viable synthetic aperture sonar led P. deHeering (deHeering, 1984) to suggest alternate suboptimal processing schemes. Two techniques he discussed are of particular interest. The first is the use of broadband processing to reduce the influence of azimuth ambiguities associated with spatial undersampling. Since the angular position of the grating lobes are frequency dependent, broadband operation smears them together. Increasing the bandwidth improves the performance of this technique. The other is to envelope process the received signal when it lacks phase coherence due to medium and platform instability. In terms of platform stability, this would reduce the accuracy required in positioning the platform by around an order of magnitude. This technique is also particularly interesting as it would reduce the incidence of specular artifacts in the subsequent

image, a significant problem with highly coherent imaging systems such as synthetic aperture sonar.

Attention has been given to the assessment of the impact of platform motion on the formation of a synthetic aperture. Work by D. Checketts and B. Smith (Checketts and Smith, 1986) at the University of Birmingham, England, analysed allowable limits in both amplitude and frequency upon six degrees-of-freedom motion. This was based upon an image quality 'figure of merit' they proposed. Experimental verification of their conclusions was not possible at the time.

Perhaps the earliest attempt at experimental verification of the operation of a synthetic aperture sonar in the ocean came from a group at the University of Christchurch, New Zealand. This effort was led by P. Gough. Their sonar was not housed in an unconstrained towfish, rather it moved along wire ropes to reduce the influence of platform motion. They described the experimentation in the paper published in 1989 (Gough and Hayes, 1989a). Unlike other systems to that date, it used continuous transmission frequency modulation (CTFM) signals to obtain a large bandwidth in the acoustic transmission. As the signals operated with a 100% duty cycle, the sonar required separate transmitters and receivers (in contrast to narrowband implementations that are 'ping' based). They successfully trialed their sonar and demonstrated its ability to image an air-filled test target off a pier in Loch Linnhe, Scotland. Particularly interesting in the results of the narrowband processing were the appearance of grating lobes from spatial undersampling, with some artifacts being stronger than the test target. They combine a number of narrowband images both coherently and incoherently, demonstrating the differences in resolution and occurrence of specular artifacts.

The New Zealand group also made measurements of temporal phase stability in a highly turbulent water column. They found the phase fluctuation to be insignificant (Gough and Hayes, 1989b). This was in the 15-30kHz frequency range over a two-way propagation path of 130m. This was lower in frequency, but at a greater range than that attempted by Loggins in the work discussed earlier.



A special edition of the IEEE Journal of Oceanic Engineering in January, 1992, devoted a significant section to synthetic aperture sonar systems. A number of papers in this edition were relevant to this discussion, particularly the tutorial paper by M. Hayes and P. Gough (Hayes and Gough, 1992). They discuss at length narrowband and broadband implementations of synthetic aperture sonar, with particular emphasis on the CTFM sonar they developed over several years. Contrasted in the article are environments that synthetic aperture radar and the sonar equivalent operate. Also, the difficulties of blindly applying the results of the former to the latter. They detail image reconstruction algorithms and plot intensity distributions that demonstrate these. The article is concluded with a discussion of a number of areas that are yet to receive attention in synthetic aperture sonar. These include techniques of speckle reduction for improving image quality and platform motion estimation from acoustic data.

An interesting article in the same edition by K. Rolt and H. Schmidt (Rolt and Schmidt, 1992) examines the occurrence of azimuth ambiguities with synthetic aperture sonar. Airborne synthetic aperture radar has a relatively high pulse repetition frequency, compared to that of sonar (in the sonar case the repetition rate generally only just satisfies the minimum to avoid ambiguities). As such, SAR images are free from spatial ambiguities. They demonstrate that spaceborne synthetic aperture radar more closely resembles the sonar application. This is because the pulse repetition frequency is more limited to that required by aperture sampling constraints. Detailed in the paper are computer simulations based upon the geometry of the experiment by Gough and Hayes, showing the appearance of azimuth ambiguities for different combinations of aperture size, centre frequency and bandwidth.

A conceptual design of an operational synthetic aperture sonar is discussed in a paper by M. Bruce (Bruce, 1992). He details the system design considerations for such a sonar, along with the operational constraints imposed on it. He bases an example system on an existing side scan sonar, the SeaMARC, and shows it is possible to achieve comparable survey rates with a finer along-track resolution. His example is less aimed at applications that require high tow speeds. The SeaMARC is a deep ocean side scan sonar and its tow speed is limited by the length of attached tow cable. Increasing the tow speed would mean that the desired depth could not be

achieved due to cable drag. Synthetic aperture techniques are appropriate in this application as the high tow speeds are not required.

A paper by J. Chatillon, M. Bouhier and M. Zakharia (Chatillon et al., 1992) as part of a European MAST project describes the relative merits of narrowband and wideband synthetic aperture systems. They develop computer simulations of both ideal and perturbed towfish trajectories, and examine processing schemes to evaluate the merits of the signal types. They draw a number of conclusions from their simulations, one being that of the advantage in using wide-band signals for synthetic apertures, regardless of the navigation performance. This is mainly due to the smearing of the beam patterns during image formation.

The use of techniques to reduce the effect of platform motion on a synthetic aperture appears in a paper by Z. Meng and J.W.R. Griffiths (Meng and Griffiths, 1993). This work demonstrates the use of the contrast optimisation, autofocusing technique. The motions described here are simple in nature and slowly changing. These motions were simulated and the differences in autofocusing performance noted for a limited range of motions. Experimental measurements were performed in test tank experiments to display the technique with targets. The work was not intended to be representative of the motions experienced in an ocean going sonar.

The combination of sophisticated inertial navigation system with autofocusing techniques in an end to end simulation is discussed in a paper by B. Huxtable and E. Geyer (Huxtable and Geyer, 1993). This is a simulation exercise where the model consists of a number of sections, being representative of an implementation of a synthetic aperture sonar. Measurements from both motion sensors and a Doppler velocity sonar are given to a Kalman filter processor for a primary motion measurement. With this primary measurement the acoustic data is phase adjusted and then processed using a seismic migration algorithm to reconstruct an image. Finally, various autofocusing techniques are applied to the image to improve its quality. Two SAR algorithms are used, a subaperture correlation algorithm and the phase gradient algorithm. They conclude that the primary motion measurement is not sufficient to produce a high resolution synthetic aperture sonar image. However, when combined with autofocus techniques high resolution images are achievable. They find that the

phase gradient algorithm produces the smallest phase error in the image reconstruction.

The first synthetic aperture sonar to be deployed in an unconstrained towfish is documented by B. Douglas and H. Lee (Douglas and Lee, 1992 and 1993). Their sonar uses a multiple element receive array (10 elements in a 1m array at centre frequency of 600kHz) and they synthesise an aperture of maximum length 6m. over a range of 125m. Of particular interest here is the very stable tow body they deploy. They assume in their processing that the tow path deviation is negligible so no direct measurement is made of it. Rather, compensation for position irregularities is made in the image formation algorithm from the acoustic data. They describe their imaging algorithm in the following steps:

1. Form a preliminary complex-valued image for each transmit pulse.
2. Align the preliminary images spatially, determining actual platform motion.
3. Apply a range dependent phase correction term.
4. Obtain a high-resolution image through complex superposition of preliminary images.

The images produced with this algorithm exhibit an improved along track resolution and superior signal-to-noise ratio than conventional sidescan imaging.

A statistical technique to overcoming motion effects in a reconstructed synthetic aperture image is discussed in a paper by K. Johnson *et al* (Johnson, Hayes and Gough 1995). They examine the different degrees of freedom in motion experienced by a tow body and conclude that the three rotations have negligible impact in a well designed towfish. Of the three translations it is only sway that is of significance and they concentrate on estimating this motion in the paper. However, in their treatment of sway motion they place the restriction that for coherent imaging the sway between adjacent samples must be less than a wavelength. They describe a speckle imaging technique that uses the statistics of the phase variations of the returned echos to determine the towfish trajectory. Rather than requiring strong point targets, it is claimed to be suitable for clutter limited images. This technique has not been verified experimentally.

The culmination of one of the activities in two large European (MAST) funded synthetic aperture sonar projects is presented in a paper by A. Adams (Adams *et al*, 1996). The group at the University of Newcastle upon Tyne designed the real time data processing for the sonar that was developed. The data processing unit consisted of a parallel array of Transputers in a pipelined architecture. Although the arrays for the project consisted of a number of individual sensors, only two channels were processed in real time. The reconstructed image results from field trials in the Mediterranean Sea are impressive in their improved clarity over a conventionally processed image. In their system it was fortunate that the tow body was sufficiently large and stable (relative to the acoustic wavelength from a centre frequency of 8kHz); motion compensation was not required. The arrays for each channel were vertically displaced from each other and this allowed the data to be processed for bathymetry.

## **Chapter 3 Theory of Synthetic Aperture Sonar**

### **3.1 Introduction**

The basic theory of synthetic apertures is well developed. Chapter 2 detailed many of the publications where this theory has been applied for radar and in the underwater environment. This chapter discusses the theory of synthetic apertures, particularly in the context of the sonar developed for this thesis. The standard results are simply stated as it is considered unnecessary to duplicate those available in standard texts on the subject. Particular attention is given to the contrasts between the constraints associated with synthetic aperture and to those of real apertures.

The ocean is a constantly changing environment through tidal and wave action. High resolution images of the sea floor can be degraded considerably by failure to account for the relative motions between the sonar and the area being imaged. This dynamic environment poses significant limitations on the application of the theory in predicting the performance of a sonar imaging system. These limitations are more severe in the case of synthetic aperture imaging. As such, the motion of the sonar must be considered in a model to predict its performance. The latter parts of this chapter develop a framework for the description of such platform motion.

Sound propagation is a complex subject and some significant simplifications are made for this discussion. To simplify the performance prediction models sound energy is assumed to take the path that is suggested by the geometry of the sonar relative to the sea floor (or line of sight), this ignores the diffractive and multi-path sound propagation encountered in reality. As the sonar described in this thesis operates only over short ranges (less than 200m) these simplifications can be justified on the basis of being representative of ideal water column conditions.

## 3.2 Synthetic Apertures

The theory of apertures is a mature field. Array theory texts (Steinberg, 1976) describe that a continuous array can be approximated by discrete elements and sampling theory used to describe the properties of this aperture. Such apertures can be either real or synthetic. The real aperture is composed of a finite number of antenna elements (hydrophones in acoustics) distributed linearly and normally sampled simultaneously in time. The synthetic aperture is formed with only a single antenna element that moves through the same locus as the real array and is sampled at the different spatial positions at consecutive instants in time.

The normalised, far field beam patterns a real array,  $F_r(\theta)$ , and a synthetic array,  $F_s(\theta)$ , (as a function of azimuth angle  $\theta$ ) have similar features, although their differences are significant.

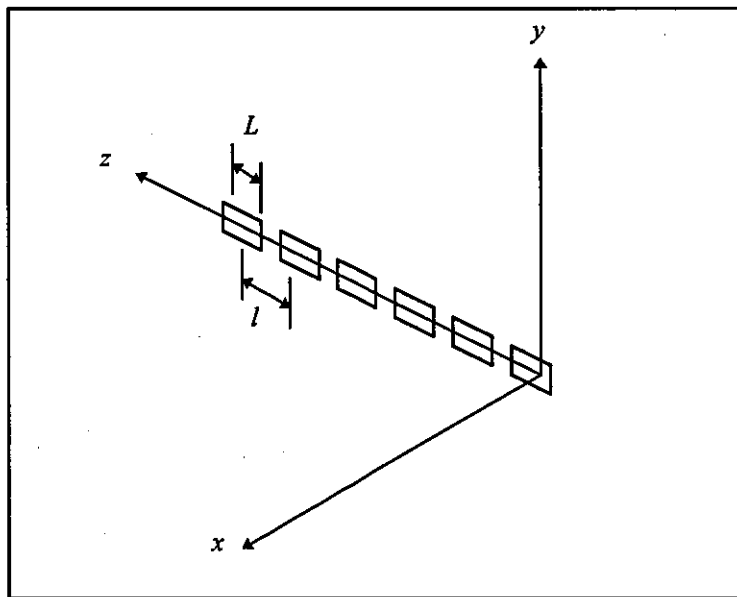


Figure 3.1 Array Geometry

Consider a real array consisting of  $N$  antenna elements of length  $L$  with spacing between centres of  $l$ . This situation is depicted with co-ordinate axes in Fig. 3.1. Each element is assumed to have the same far field beam pattern  $F_e(\theta)$ , corresponding to a

complex excitation  $f_e(z)$  at each element position. By summing the individual complex excitations over the  $N$  elements we determine the array response to be :

$$f_r(z) = \sum_{n=1}^N f_e(z - nl)$$

Assuming a narrowband signal of wavelength  $\lambda$  incident on the array, this expression can be alternatively expressed in the form of a normalised, far field beam pattern  $F_r(\theta)$ , where:

$$F_r(\theta) = F_e(\theta) \frac{\sin[\Pi N(l/\lambda) \sin\theta]}{N \sin[\Pi(l/\lambda) \sin\theta]}$$

In contrast, rather than  $N$  antenna elements, a single element traverses the same total length and creates a synthetic aperture in doing so. The normalised unfocused synthetic beam pattern in this case is:

$$F_s(\theta) = F_e(\theta) \frac{\sin[2\Pi N(l/\lambda) \sin\theta]}{N \sin[2\Pi(l/\lambda) \sin\theta]}$$

Note the appearance of the factors of 2 in both the numerator and denominator. This is a consequence of the path lengths to a target changing twice as quickly with position; as the single antenna acts as both transmitter and receiver.

The beamwidth in both cases can be found by examining the behaviour of the numerator. This goes to zero when the bracketed component is a multiple of  $\Pi$ . We are interested in the angular position when this occurs the first time as this gives the width of the main lobe (null to null beamwidth). For the synthetic aperture case this becomes:

$$\theta = \sin^{-1}\left(\frac{\lambda}{2NI}\right)$$

This expression is half that for the real array, so the beamwidth narrows by a factor of two in the synthetic case. This implies that a synthetic aperture needs only be half the length of the real array to achieve the same beamwidth performance.

The behaviour of the denominator of the beamwidth expressions is also significant. When this goes to zero the total expression is undefined. This corresponds to the

appearance of grating lobes in the array response. For the synthetic case, if  $l > \lambda/4$  grating lobes will appear in the visible angular range  $-\pi/2 < \theta < \pi/2$ . Comparing with the real array case, this implies that a synthetic aperture has to be spatially sampled twice as frequently as a real array to avoid azimuth ambiguities in the resulting image.

The effect of the finite beamwidth of the synthetic array element has not been considered in this discussion. If the synthetic aperture is sampled less frequently than  $\lambda/4$  grating lobes will appear at a visible azimuth angle from broadside. However, if the array element is of appropriate length then a null in its beam pattern can be placed at this azimuth angle. The result is that the grating lobe is removed, or at least reduced to a level that it will not be apparent in the image. An often quoted result associated with this is that a synthetic aperture must be sampled at  $L/2$  or greater. This is an interesting result as it is independent of frequency.

The discussion has compared the characteristics of far field beam patterns for both real and synthetic apertures. However, for the latter we generally wish to operate in the near field region. This allows focusing of the array and improved resolution (the same principle can be performed on real arrays). The derivation of an analytic expression for the near field beam pattern is a complex calculation, well beyond the scope here. In reality the grating lobes of a synthetic array are not completely suppressed by the element response as would be expected from the far field theory. For the sake of this discussion the grating lobe reduction is sufficient for the purpose of imaging.

### **3.3 Synthetic Aperture Resolution**

The resolution cell of a sonar image can be described in terms of two orthogonal axes, one in the across track direction (azimuth) and the other in the along track. In the across track direction no improvement in resolution can be achieved through synthetic aperture processing. The characteristics of the transmitted signal and the detection process govern this. In the along track direction synthetic aperture processing offers considerable improvements to resolution.



The azimuth resolution is the width of the main lobe at which two adjacent targets can be distinguished. Borrowing from astromomers this is usually stated as a 3dB drop in the array respose being the minimum necessary to distinguish the two. This criteria is also adopted in underwater acoustics.

The beamwidth of an array and its azimuth resolution are closely linked. Already mentioned has been the null-to-null beamwidth of an array. A nominal angular resolution,  $\theta_R$ , is usually defined as the 3dB beamwidth of an array. For a real array (of total length  $L_R$ ) this is found to be:

$$\theta_R = \sin^{-1}\left(0.44 \frac{\lambda}{L_R}\right) \approx 0.88 \frac{\lambda}{L_R} \approx \frac{\lambda}{L_R}$$

The azimuth resolution,  $\Delta z_R$ , for a real array is a function of range,  $R$ , and increases proportionately with it. This is defined by:

$$\Delta z_R \approx R\theta_R:$$

As a consequence, the beam spreads with range. The image will show targets of the same physical dimension increasing in azimuth width the further they are from the sonar.

This has identified the far field resolution, but not the near field resolution of an real array. The resolution in the near field can be sufficiently approximated by the array length  $L$ .

The resolution of a synthetic array differs from the real array. Consider an individual antenna element of length  $L$  that has a beamwidth  $\theta_p$ . This element forms a synthetic array of length  $L_s$  and beamwidth  $\theta_s$ , where:

$$\theta_s \approx \left(\frac{\lambda}{2L_s}\right) \tag{a}$$

To achieve a resolution of  $\Delta y_s$ , at a range  $R$  the beamwidth of the synthetic aperture must be:

$$\theta_s \approx \left(\frac{\Delta y_s}{R}\right) \tag{b}$$

However, the point at range  $R$  must be in the real beamwidth  $\theta_B$  of the element over the entire synthetic aperture length, so:

$$\theta_B \approx \left(\frac{\lambda}{L}\right) = \left(\frac{L_s}{R}\right) \quad (c)$$

Substituting the expression (c) for  $L_s$  into (a) and equating (a) and (b) we are left with:

$$\Delta y_s = \frac{L}{2}$$

The resolution of the synthetic aperture is constant and dependent only upon the size of the individual element. This is an interesting result and in complete contrast to the result for a real array. The resolution of a real array can be improved by increasing the operating frequency and/or increasing the array length. Neither of these have any influence in synthetic aperture processing.

### 3.4 Ambiguities

Ambiguities result in a degradation of sonar images. Regardless of whether these images are produced from either synthetic arrays or real arrays the sampling constraints must be met. Images from synthetic arrays are more susceptible to degradation due to the higher aperture sampling rates they require. Ambiguities are to be avoided, or at least their impact minimised as much as possible. Both range and azimuth ambiguities are examined here and the typical constraints they impose demonstrated.

#### 3.4.1 Range Ambiguities

Range ambiguities manifest themselves as an inability to distinguish the range at which a particular target echo is received. Range ambiguities are avoided with only one acoustic pulse in the insonified area at any given time. If the restriction of only one such pulse is made an expression for the pulse repetition rate can be determined. A maximum range  $R_{\max}$  is defined as the distance from the sonar at which a returned signal is reduced to a negligible intensity. If the sound propagation velocity in water is

$c$ , then the time between pulses is  $t_{\max} = 2R_{\max} / c$ . Hence, the maximum pulse repetition frequency is:

$$v_{\max} = \frac{c}{2R_{\max}}$$

For a maximum range of 200m the maximum repetition rate is 3.75Hz.

This condition can be relaxed with the use of distinguishable signals. These different signals could be either narrowband or broadband. In the narrowband case, different frequency transmissions would suffice, provided that narrowband filters can distinguish them. In the broadband case, different phase coding of the signals would make them distinguishable.

### 3.4.2 Azimuth Ambiguities

Grating lobes from spatial undersampling manifest themselves as azimuth ambiguities. In our discussion of synthetic aperture beam patterns it has been noted that the synthetic array must be spatially sampled at intervals of  $\lambda / 4$  or less to avoid the occurrence of grating lobes. This imposes a constraint on the maximum speed at which the sonar can traverse the aperture.

If the maximum range of a sonar is  $R_{\max}$  and sound propagation velocity is  $c$ , the time between subsequent pulses is once again  $t_{\max} = 2R_{\max} / c$ . Let us assume that the sonar is constrained to travel no further than  $\lambda / 4$  between pulses to avoid azimuth ambiguities. The maximum velocity of the sonar is given by:

$$v_{\max} = \frac{\lambda c}{8R_{\max}}$$

For a range of 200m and an operating frequency of 80kHz a maximum towing speed of  $0.02\text{ms}^{-1}$  results, an unacceptably slow tow speed. Techniques of increasing the tow speed are thus necessary for a practical implementation of a synthetic aperture.

Our discussion has not accounted for the grating lobe suppression associated with the finite real beamwidth of a synthetic array element. The aperture sampling frequency is

reduced due to this. In this case the array must move no further than  $L/2$  between pulses. The maximum velocity can then be found to be:

$$v_{\max} = \frac{Lc}{4R_{\max}}$$

This reduces the spatial sampling requirements provided that the array elements are sufficiently long. For a more realistic tow velocity of  $2\text{ms}^{-1}$  an array 1.9m in length would be required. However, an array of this length is both difficult and expensive to fabricate.

### **3.5 Area Mapping**

The discussion has demonstrated the spatial sampling constraint imposed on a synthetic aperture sonar. This is a severe limitation and results in a sonar velocity that is considerably slower than that acceptable in a practical system. As such, it is important to consider techniques for relaxing it. A number techniques have been proposed and a selection of these are given in this section.

#### **3.5.1 Multiple Vertical Beams**

With multiple vertical beams a number of distinguishable acoustic beams insonify adjacent areas of the sea floor at the one time. This technique can be envisaged as having a number of synthetic sonars operating in parallel at the one time, with the beams being produced from separate arrays. Potentially the increase in tow speed is proportionate to the number of beams.

The multiple beams could be the same centre frequency. If they were then careful beam footprint design would be necessary to remove any ambiguity as to the source of each waveform. The beam footprint limitations could be relaxed with the use of sufficiently distinguishable signals being produced from each array. As already noted these could be either narrowband or broadband. The source of each signal would be known and only those from the same source coherently integrated for each array.

### **3.5.2 Multiple Receive Elements**

Implementing multiple receive elements is a simple technique for increasing the tow speed. This is often referred to as vernier processing. An implementation of this technique consists of a single transmitter and multiple receive elements. The single transmitter produces a pulse and this is received on all receiving hydrophones. The increase in tow velocity is proportionate to the number of hydrophones utilised. The resulting image does not suffer from ambiguities provided that care is taken with the placement of the receive elements and aperture sampling constraints are respected. The disadvantage here is the additional hardware and data associated with the extra signal channels.

### **3.5.3 Broadband Operation**

Broadband operation can relax the spatial sampling constraints. As the azimuth directions of grating lobes are frequency dependent, integrating over a range of frequencies tends to smear the grating lobes; whilst reinforcing the main beam. The integration is a matched filtering process that rejects random noise so the signal to noise ratio improves with such a technique.

A variety of broadband signals are available. The most common of which is the CHIRP, although phase coding of pseudo random sequences is also available.

## **3.6 Motion Compensation**

A towfish in the ocean follows a path through the water that deviates from the ideal straight and level trajectory of uniform velocity. The driving forces on the towfish are the motion of the vessel acting through the tow cable and the motion of the surrounding water mass. The water mass can subject the towfish to surging motion from the ocean swell and to constant velocity offsets from tidal currents. The cable from the vessel will force cyclic motions on the towfish as cable tension varies. The

combination of these and other potential motion perturbations result in the towfish experiencing a complex trajectory.

The motion of a towfish can be uniquely described by three translations and three rotations, with these acting about orthogonal axes. The translations move the entire body uniformly, while the rotations are presumed to act about its centre of rotation (in this case the tail fins act to constrain the motion, so this centre will be at the rear of the body). The three translations are sway, heave and surge as shown in Figure. 3.2, along with the three rotations of pitch, yaw and roll. This diagram depicts the towbody as a local coordinate system (x,y,z) within global coordinates (X,Y,Z), the latter being fixed in space.

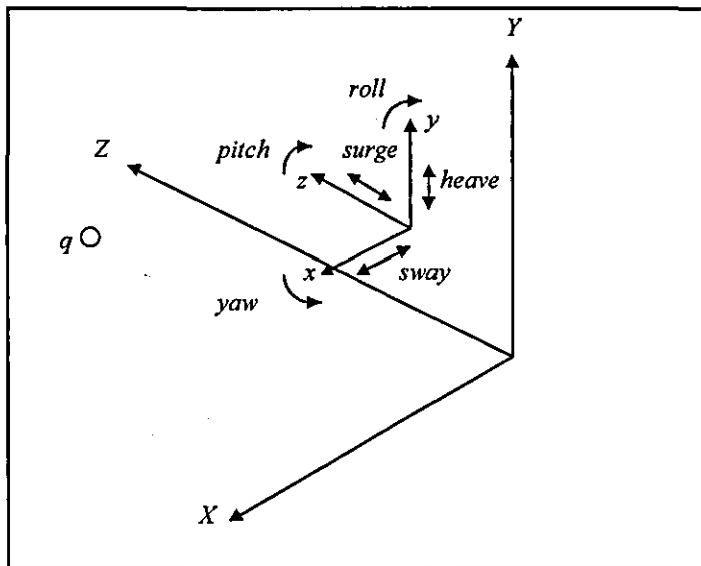


**Figure 3.2** Towfish Motions Relative to Fixed Co-ordinates

The relative position of a point on the seafloor from a towfish experiencing a complex trajectory is of interest here. From the geometry depicted in Figure 3.2 it is possible to develop an expression for the position of a point on the sea floor relative to the towfish.

The position of the origin of the towfish in the global coordinates at time  $t$  can be represented by the vector:

$$p(t) = \begin{bmatrix} X(t) \\ Y(t) + h_o \\ Z(t) + V_o \cdot t \end{bmatrix}$$

Where  $h$  is the height above the sea floor and  $V$  the constant forward velocity of the ideal towfish trajectory.

If the position of a point on the sea floor in the global coordinates is  $q$ , then this point in to the towfish coordinates is given by  $q - p(t)$ . If the towfish is subject to angular motion then the position of the point on the seafloor becomes:

$$q'(t) = T(t)\{q - p(t)\}$$

where the transformations  $T$  for the single angular displacements of pitch (rotation about x-axis), yaw pitch (rotation about y-axis) and roll pitch (rotation about z-axis) are respectively given by:

$$\begin{bmatrix} 1 & 0 & 0 \\ 0 & \cos\alpha & -\sin\alpha \\ 0 & \sin\alpha & \cos\alpha \end{bmatrix}, \begin{bmatrix} \cos\beta & 0 & -\sin\beta \\ 0 & 1 & 0 \\ \sin\beta & 0 & \cos\beta \end{bmatrix}, \begin{bmatrix} \cos\gamma & -\sin\gamma & 0 \\ \sin\gamma & \cos\gamma & 0 \\ 0 & 0 & 1 \end{bmatrix}$$

A general transformation requiring all three rotations requires an ordering convention to be unique. Performing yaw, followed by pitch and finally roll transformations gives the general transformation:

$$T = \begin{bmatrix} \cos\beta \cos\gamma + \sin\alpha \sin\beta \sin\gamma & -\cos\alpha \sin\gamma & -\sin\beta \cos\gamma + \sin\alpha \cos\beta \sin\gamma \\ \cos\beta \sin\gamma - \sin\alpha \sin\beta \cos\gamma & \cos\alpha \cos\gamma & -\sin\beta \sin\gamma - \sin\alpha \cos\beta \cos\gamma \\ \cos\alpha \sin\beta & \sin\alpha & \cos\alpha \cos\beta \end{bmatrix}$$

This discussion has developed a general expression for the position of a point on the seafloor relative to the towfish as it follows a non-ideal path through the water. With knowledge of the variation in position and variation of aspect from the ideal it is possible to adjust the received acoustic signals in both phase and amplitude to compensate.

# Chapter 4 Experimental Synthetic Aperture Sonar

## 4.1 Introduction

The synthetic aperture sonar developed for this study consists of both an underwater platform and surface electronic equipment. The equipment is shown in Fig. 4.1. The platform is towed behind a vessel and incorporates both an acoustic section and motion measuring equipment. Aboard the vessel is the computer controlled data recording system. This surface equipment is split into two systems, one records acoustic data from the sonar while the other independently receives motion data. The data recorded from both sources is combined and processed at a later stage to produce high resolution images of the sea floor.

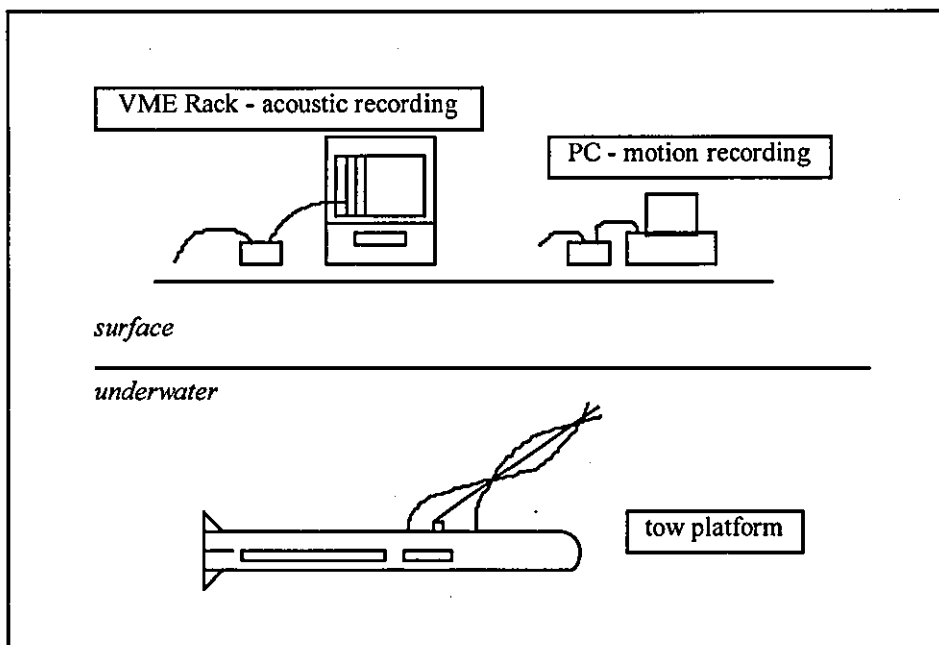


Figure 4.1 Synthetic Aperture Sonar System

The sonar designed and fabricated for this thesis is intended as a research tool. As such, an effort was made to reduce the complexity in both construction and operation. A result of this is that it only images to one side of the towfish. This reduces the number of acoustic elements and the amount of data produced. Another consequence is that it does not have sufficient computational power to produce images of the sea



floor in real-time. All acoustic and motion data is recorded in a raw format for processing at a later date.

The towfish is divided into two separate sub-systems. The first is the acoustics section (acoustic receivers and transmitters, with associated electronics). The second is the platform motion measuring equipment. Both reside within separate compartments in the towfish, with the motion equipment in the front. The motion equipment is conveniently housed in the body of a commercially available towfish; the Klein Associates Inc. Model 595. The acoustics section is integrated into a purpose built canister that extends the overall length of the towfish and is of slightly greater diameter than the 595 body. The original fin assembly is still used, although it is set further back behind the new body section. A photograph of the towfish assembly is shown in Fig. 4.2.

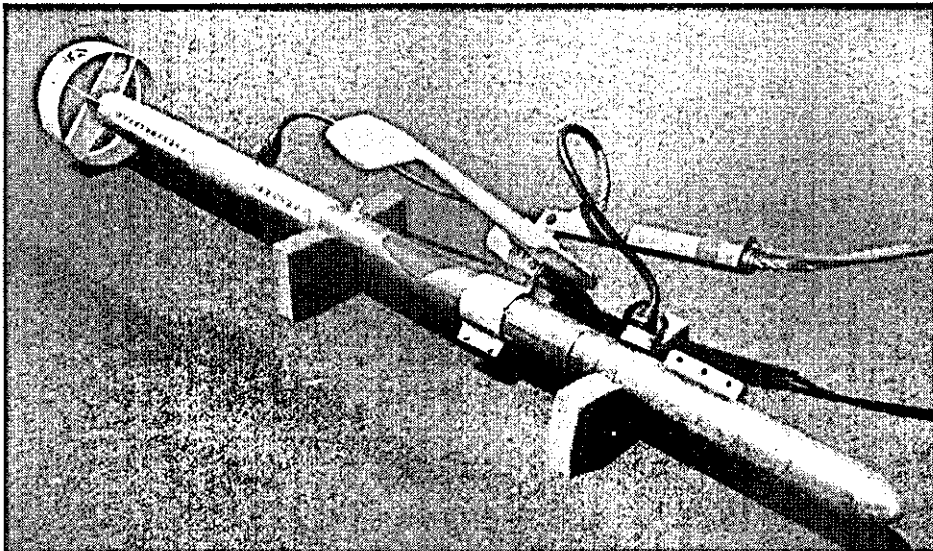


**Figure 4.2**      **Towfish Assembly**

The surface vessel electronics for the acoustic section comprises a data recording system and a transmit waveform generation system. The data for this section is received and reformatted on a VME card, then recorded on a high bandwidth video recorder. Integrated in the VME rack is a control card that produces transmit timing and generates digitally synthesized waveforms. These transmit waveforms are amplified on the surface and transmitted on the underwater transducers.

The motion recording system was independently designed and fabricated for another project. It had been used to a limited extent for assessing the dynamic behaviour of underwater equipment. Being able to reuse this system saved both expense and time for this work. Modification of the equipment was required for this project. It required new interface cabling and new software to communicate synchronization data between the two data recording systems. As this piece of the system is not original to this work it is not discussed in depth. However, the data recorded from it is of considerable interest and this is presented in detail in subsequent chapters. All data processing is original to this work and is discussed in detail.

The motion data takes a separate path to the acoustic data when recorded on the surface vessel. It passes up a separate cable and through a reformatting module. The translated data is subsequently recorded on a PC hard disk.

In contrast to the motion measuring equipment, the acoustic section of the towfish and the associated surface electronics is original for this research. This includes the electronics and the specialised housing for the towbody. The surface electronics includes two complex electronic circuit cards and the associated control software. The effort in design and fabrication of this part of the system was considerable. The transducers, electronics and software were designed and implemented by the author, while the mechanical housing was produced under supervision to the desired specification.

## **4.2 Overview**

The motion measuring system consists of an underwater package mounted in the nose of the tow body and some surface vessel mounted recording equipment. The underwater package consists of two sections, a six degree-of-freedom (6DOF) measurement system and a static sensor (SS) package. The 6DOF system consists of three accelerometers and three gyroscopes arranged on orthogonal axes. Such a configuration allows the trajectory of the body to be uniquely defined. The SS package consists of a depth pressure gauge, a low frequency roll sensor, a low

frequency pitch sensor and temperature transducer, these are ancillary measurements to those produced by the 6DOF. The data from both packages is multiplexed onto the one serial link and transmitted to the surface on a dedicated cable.

The underwater motion package interfaces to associated equipment on the surface vessel. This equipment provides the power supply and data recording on a PC. The PC associated with this equipment produces synchronisation data words on its parallel port. These are recorded with both the motion data (on the PC) and the acoustic data on the video recorder. This synchronisation gives a coarse two second granularity in the time matching of the two data sets. A finer resolution time stamp would have been more desirable had it been possible.

The acoustics section consists of the underwater transducer data collection package and the surface vessel recording/control package. As an active sonar it is 'ping' based, an acoustic waveform is transmitted at regular intervals whilst sensors simultaneously collect echo returns from underwater objects. The control processor in the surface VME rack regulates the timing of these transmissions and digitally synthesises the transmit waveforms.

The communications between the surface and the underwater platform for the acoustics section is over a dedicated multi-conductor cable. The amplified transmit waveforms are transmitted down the cable array on several conductors. In the opposite direction digital data that has been collected from the elements of the receive array are sent to the surface on other conductors. In addition to these functions, the cable provides power for the underwater electronics.

Sonar data is recorded on the surface vessel using a VME computer chassis and a mass storage device called the Very Large Data Store (VLDS) from Honeywell. Two specially designed circuit cards provide the necessary interfaces for collecting data and generating transmit waveforms. The entire operation is controlled and monitored by a VME processor card running the OS/9 real-time operating system. In addition to the data collection facility, data is also reproduced using the same system.

The data recorded onto the VLDS consists of the acoustic signals, platform motion synchronisation data and transmit pulse flags. The acoustic data is FIFO buffered and rate translated (with padding words) to the synchronous rate expected by the recorder. Inserted in this stream are the regular synchronisation words from the motion recording PC. Also inserted are the transmit pulse flags that originate in the VME chassis from the triggering of the transmit pulses.

The VME computer chassis was chosen as a standard architecture due to the availability of circuit boards and the relative ease of prototyping for the design of any specialised ones. The VME processor card was purchased as a standard piece of hardware with the OS/9 already ported to it. It was a matter of loading the operating system onto hard disk and a development system was immediately available.

The VLDS was the only high bandwidth data recorder available when this project began. It uses rotary helical-scan technology to record digital data onto a videotape cartridge. The videotape is a specialised version of the commercially available VHS format; it can store up to 10.4 Gbytes of data (for a 120 min. tape). Of particular interest in this application is the sustained high data rate of 4 Mbytes/sec, with byte wide data able to be recorded and reproduced on two separate channels.

The first of the purpose built cards provides an interface to the VLDS, it is called the VLDS/IF for VLDS Interface. This card incorporates two bus standards, the VME and the VSB, whilst also allowing for the peculiar VLDS interface. Commands for the VLDS are written to the VME bus by the host processor card. These commands are FIFO buffered and translated into the relatively slow format that the VLDS requires. When data is reproduced from the VLDS this card provides alignment onto 4 byte word boundaries for block transfer across the VSB bus to a dual-ported memory card.

The second purpose built card provides a number of functions and is called the MPI for multi-purpose interface. Acoustic data that comes from the towfish is demultiplexed and translated into a byte wide format for writing to the VLDS. Multiplexed into this data stream is a nibble of motion synchronisation data and a nibble of transmit synchronisation. The MPI has a digital to analogue (D/A) converter that creates the transmit pulses from a data buffer after triggering. The buffers are

created by the host processor and downloaded to the card across its VME interface. The trigger for the transmit pulse is received on the front panel from a function generator. The transmit pulse is not amplified on this circuit card. The output of the D/A converter is amplified in a commercial power amplifier before cable connection to the transmit transducers.

A photograph of the surface vessel recording systems is given in Fig. 4.3. The VME recording system and VLDS recorder are in the transport case on the right of the photo. The power amplifier for the acoustic transmissions is on the left. The PC motion recording system is sitting on top of the two transport cases, with the signal conditioner on the right.

There is a further circuit card that was designed and produced for this work, it is part of the underwater sonar system. This narrow card is fixed into the underwater housing and it collects the acoustic data for transmission to the surface. Signals from all six hydrophones are individually amplified, conditioned and digitised on this card. The resulting data from each is multiplexed onto a serial link and transmitted to the MPI card on the surface.

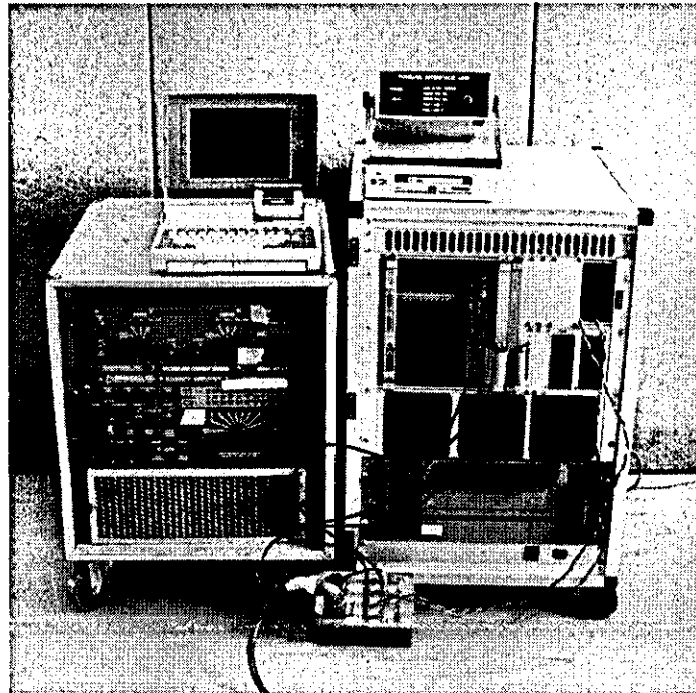


**Figure 4.3** Surface Recording Systems

### 4.3 Motion Measurement Equipment

The underwater motion measuring system consists of a number of transducers, including gyroscopes, accelerometers, depth gauges and other sensors. There are three accelerometers and three gyroscopes mounted on orthogonal axes and these sensors comprise the 6DOF measurement system. These sensors are sampled at 50Hz and they can measure motions up to the Nyquist frequency of 25Hz. Supplementing them are the static sensors for roll and pitch. These can only measure motions up to a frequency of 1Hz.

The data of most interest here is that generated by the 6DOF measurement unit. This represents both linear accelerations and rotational velocities of the underwater housing about the three orthogonal axes. From these measurements it is possible to determine the spatial positions of arbitrary points on the tow body at consecutive points in time. Acceleration data is doubly integrated to produce linear displacement, while rotational velocity measurements are integrated to obtain angular displacements of the housing.

The accelerometers were manufactured by Schaevitz (Model A215). They are of a mass-spring arrangement with a maximum range of  $\pm 5g$  (where  $1g$  is equivalent to the gravitational acceleration at sea level, that is,  $9.8ms^{-2}$ ). All three accelerometers are of the same type and have calibrated sensitivities. When placed in the housing the one that is aligned to the vertical direction has a  $1g$  offset. As the body rotates this offset is shared proportionately between all accelerometers with a component of their sensitivity in the vertical direction. The outputs of each accelerometer are separately sampled with 12 bit digitisers at a rate of 50Hz. This digitisation produces quantisation noise of  $0.0098g$ , which is similar to the  $0.01g$  inherent noise floor of the devices. A digitiser with improved resolution would have improved the quality of the collected data and would have been substituted had they been readily available.

The gyros are a solid state device and are manufactured by GEC Avionics. They have a maximum range of  $\pm 50^\circ/sec$ . These are again digitised to 12 bits of resolution at a

rate of 50Hz. This gives a quantisation noise level  $0.098^\circ/\text{sec}$ , compared to an absolute device resolution of  $0.03^\circ/\text{sec}$ . Again digitisation with better resolution would have been desirable.

Data from half a second of measurements is buffered in the underwater housing before transmission to the surface. A micro-controller in the canister reads twenty-five measurements from each of the 6DOF transducers and a single measurement from each of the SS transducers. The data is transmitted on an RS-485 link in a character format to the surface. A parity bit is added to each byte to give an indication of data integrity over the transmission. Due to the reasonably high data rates there is no facility for re-transmission of corrupt data.

At the surface the electronics package receives motion data. It also provides power for the underwater package. The RS-485 format is translated to RS-232 and the data transferred on another serial connection to a PC. The PC writes this data to hard disk in a raw format. With each block of data it writes it also includes the synchronisation word that is available at its parallel port. The raw data is extracted at a later stage for calibration and subsequent processing.

#### **4.4 Acoustic Sensors**

The acoustic sensors used for this experimentation are of particular interest due to their broad bandwidth design. In general, most underwater acoustic sensors are reasonably narrowband. A narrowband sensor has better sensitivity (as a receiver) and increased source level (as a transmitter) than a broadband sensor over a narrow frequency range. However, both diminish rapidly away from this centre frequency. The broadband sensor will not be as sensitive at the centre frequency, but will be more sensitive over frequencies adjacent to this with the response tapering off less rapidly.

A broadband transducer is desirable in this application to examine the properties of different types of signals in a synthetic aperture sonar. With such a transducer the sonar is not restricted to just narrowband signals centred at a particular frequency.

Scope exists for using various modulated broadband signals, including 'chirps' and pseudo random phase encoded bit sequences.

There is considerable skill and experience required for transducer design and fabrication. A number of papers have been published in the area (Smith and Gazey, 1984). However, reference to these is not usually sufficient to produce sensors that perform well. Considerable trial and error is required to perfect a fabrication technique, particularly with the composition and mechanical shaping of the elements. The various types of transducer designs and their relative merits are not discussed here. Rather, the quarter-wavelength matching layer type of transducer implemented for this project is described.

The transducers are based upon ceramic disks manufactured in the material PC4D. They were produced by a company in Wales to the desired physical dimension and resonant frequency. These disks have resonant modes in both thickness and radial directions. It is the lowest frequency thickness mode resonance that is of interest and the original intention was to have this as close to 68kHz as possible. (A reasonably high frequency was desired for good range resolution, though not so high as to require expensive analogue to digital conversion circuitry). However, the manufacturing process has restrictions and a limitation in the disc length was necessary for mechanical stability. The discs were manufactured in a diameter of 21mm and length of 21mm, giving a resonant frequency of about 67kHz. A larger diameter would have been preferable, though this was not physically possible if the desired resonant frequency was to be maintained (the disc would have been too long for mechanical stability).

Placed between the ceramic and water is a quarter-wave head as shown in Fig. 4.4. The head is designed to match, at the resonant frequency, the relatively high acoustic impedance of the ceramic to the lower impedance of water. The increase in load on the ceramic increases the bandwidth of the final transducer. There is a compromise between bandwidth and sensitivity, so by increasing the bandwidth the sensitivity is reduced. The head also provides a convenient place to water seal the ceramic. An 'O' ring is placed on the head between it and the housing.



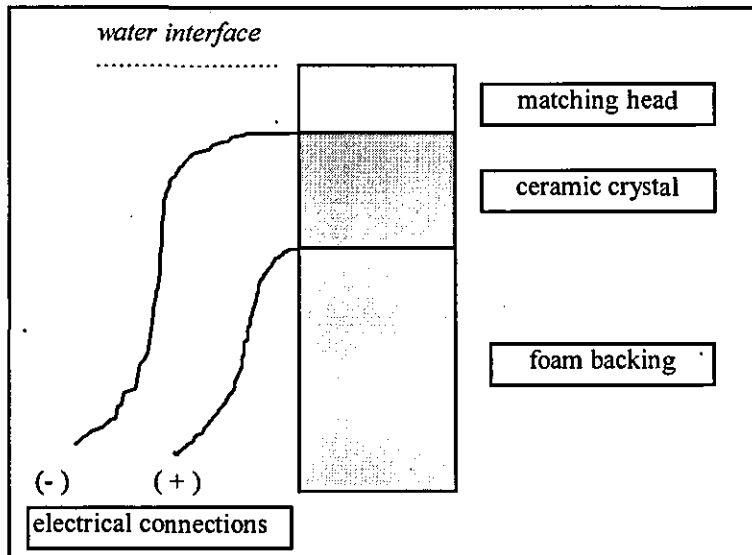


**Figure 4.4 Acoustic Sensor Construction**

The quarter-wave head in this case was produced from epoxy resin loaded with an aluminium powder. These are mixed in a ratio of 1:1 by volume. This gives a characteristic impedance of 5.3 Mrayls which is close to the desired value, this being midway in a geometric series between that of water and the ceramic. The optimum thickness of the head for the resonant frequency is required. This could only be determined by painstakingly reducing its thickness whilst measuring the conductance of the ceramic in both air and water. The optimum thickness is found when the response in measured water is close to flat.

Placed on the opposite side of the ceramic disc is an absorbent layer. This layer is of closed cell foam that dissipates some of the acoustic energy passing through the crystal. It reduces an incident signal by 6dB after an inch of travel, with a total of 20dB being obtained in this design from the dual path length through the foam.

A disadvantage of this design is the high input impedance of the transducer, this is particularly so for the high frequency elements used in this design. A consequence of this is that high input voltages are necessary for creating a transmit pulse. A second disadvantage in the construction technique is the restriction in depth of operation unless pressure compensation is available for the canister.

The final transducers were tested in a tank and their responses recorded, the source level and receive sensitivities as a function of frequency are displayed in Fig. 4.5. Of interest here is the frequency range of 50kHz to 80kHz over which their responses are reasonably constant.

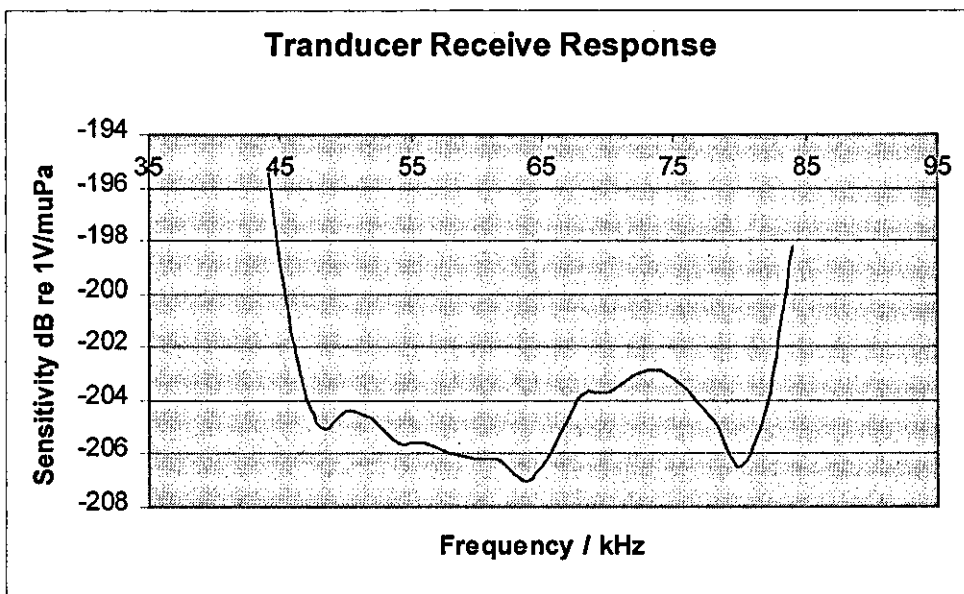
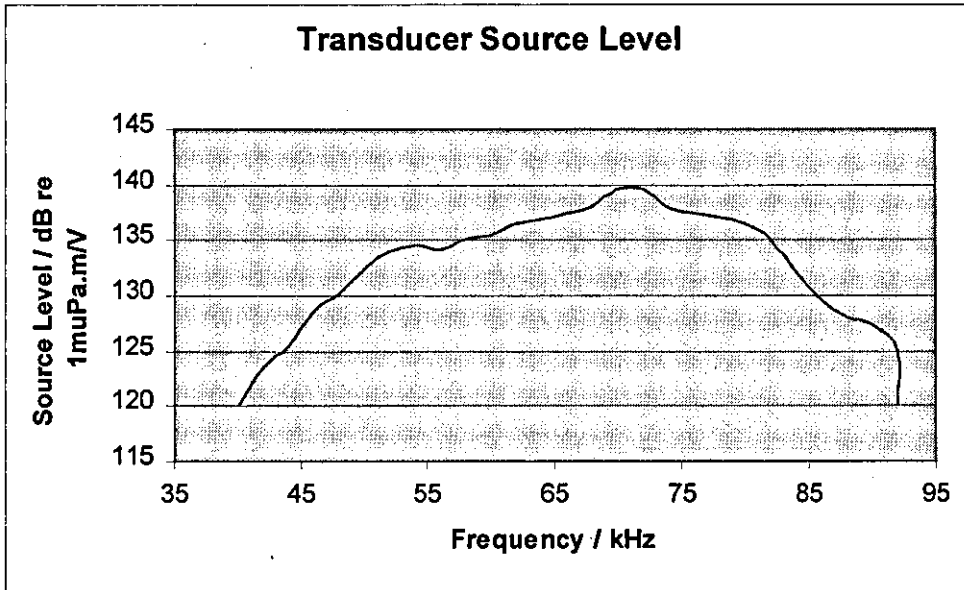


Figure 4.5 Responses of Broadband Transducers

## 4.5 Acoustic Sensor Arrays

The arrangement of the transducer elements into an array produces a beam pattern of desired shape. The array improves sensitivity in the steered direction, whilst reducing it away from this angle. In the context of the synthetic aperture sonar the use of multiple receive arrays or multiple sensors allows an improvement in area mapping rates through vernier processing. Using vernier processing the single sensor aperture sampling rates can be improved proportionally to the number elements.

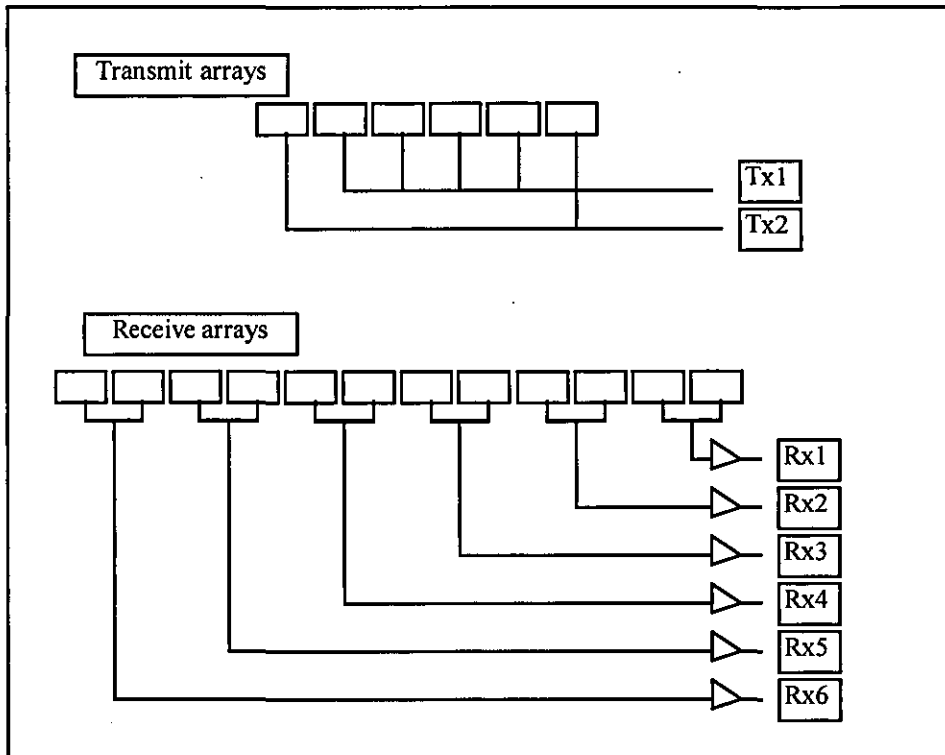


Figure 4.6 Configuration of Transmit and Receive Arrays

The experimental sonar has two separate linear arrays, one for transmitting signals and the other for receiving. The receive array consists of multiple sub-arrays. Both receive and transmit arrays use the same transducer elements as already described. The elements are secured into the housing with O-ring seals and a mounting plate is fixed to the foam backing layer. Such a construction restricts the depth of operation of the sonar to a level where the foam layer does not compress significantly and allow water entry around the head. The exterior surface of the sensors is covered with a thin film of epoxy. This epoxy affords some protection from the sea environment and is

acoustically transparent (approximately the same impedance as water). As such, it does not interfere with the signals of interest.

The transmit array consists of six elements in two sub-arrays; with each element spaced 25mm between centres. Refer to Fig. 4.6 for a diagram of both the transmit and receive arrays. Four of the elements form one array, with the extra element on each side of this array forming the other. By varying the amplitude of the transmit signal applied to the outer array it is possible to have a uniform beam width over the 50kHz to 80kHz frequency range. At 50kHz the full amplitude signal is applied to the outer array, while at 80kHz no signal is applied. This arrangement produces a beam width of approximately  $20^\circ$  across the range of frequencies. The array was tank tested and a plot of the beamwidth as a function of azimuth angle at a 70kHz frequency is given in Fig. 4.7. This plot demonstrates the source level of the array with respect to azimuth angle using all six elements in the array with equal signals applied to each.

The receive array has the same element spacing as the transmit array. It consists of twelve elements in six sub-arrays. Each sub-array pair is connected in a parallel configuration to independent amplifiers and digitising electronics. An effort was made in the selection of the receive elements to maintain pairs of approximately the same sensitivity. This ensures that they are most responsive in the broadside direction. The receive arrays were also tank tested. The source level when used as a transmitter (with all twelve elements) at 70kHz is also given in Fig. 4.7. This displays the source level with respect to azimuth angle. The existence of a grating lobe at  $55^\circ$  is evident from this plot.

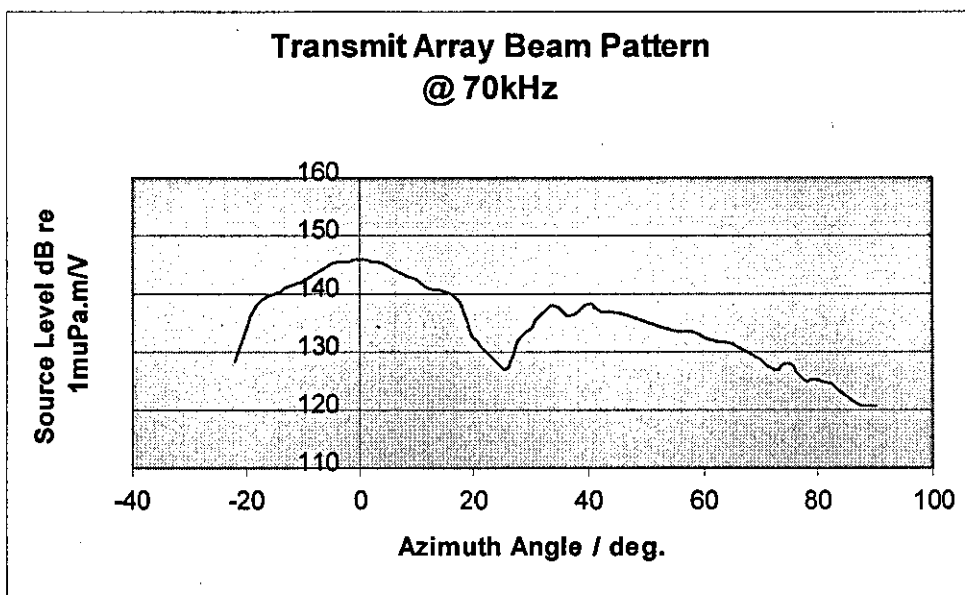
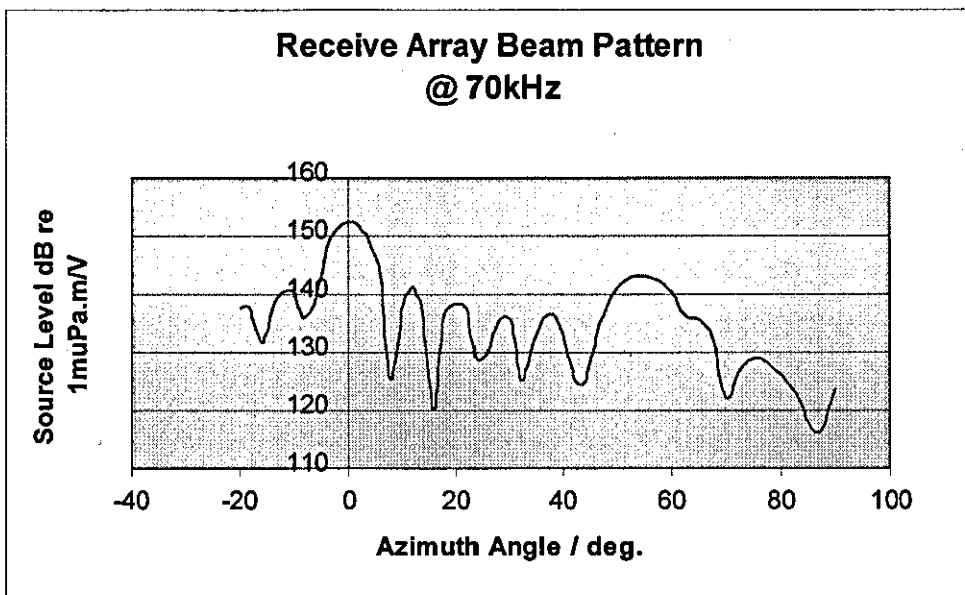


**Figure 4.7**      **Response of Receive and Transmit Arrays**

## 4.6 Acoustic Sensor Electronics

The acoustic sensors are divided between separate transmit and receive arrays. This enables echos to be detected on the receivers whilst simultaneously transmitting. As a consequence of this the transmit waveforms can have a duty-cycle of arbitrary duration. As the transmit pulse is both generated and amplified on the surface, very little hardware is required for the transmit array in the underwater housing. Only a transformer is necessary to match the relatively high transducer impedance to the low cable impedance and to obtain maximum power transfer.

The signal conditioning is more complicated for the receive array. In order to reduce the electrical cross-talk of the analogue sensor signals, the signals from each receiver are digitised as close as possible to the transducer. Rather than analogue signals being transmitted up the cable over multiple conductors, digital data is sent on a single multiplexed serial stream. The digitisation is continuous whilst power is supplied to the electronics from the surface. Digital data and synchronisation pulses are sent continuously with no facility for re-transmission of corrupt data.

Analogue sensor signals are buffered and amplified with 6dB of gain prior to being input to an analogue to digital converter (ADC). Each acoustic centre (two transducers) has its own ADC that digitises the signal to 16bits. These converters have a word throughput of 160kHz, giving a Nyquist frequency of 80kHz. As such, the bandwidth of interest extends from 0 to 80kHz. Other techniques such as quadrature sampling were considered for reducing the amount of data through the system. However, the large bandwidth of the signals of interest meant that the data reduction would not have been significant. The baseband method was adopted as the most suitable for its relative simplicity. ADCs were found to be a limiting factor in the sonar design. Higher sampling frequencies would have required very expensive components and were thus avoided. A larger dynamic range would have been desirable, however, the technology for this is not readily available at these sampling frequencies. No anti-aliasing filtering is used in the design as the signals of interest are of considerably greater amplitude than any interfering signals.

A Xilinx field programmable gate array (FPGA) controls the ADC triggering and subsequent data transfer over the serial link to the surface. The digital output of the six ADCs are time multiplexed onto a common bus and the data from each accessed sequentially as 8bit words. The FPGA converts the 16bit words into a 16Mbit serial bit stream that is transmitted to the surface electronics. One word from each ADC is transmitted after the previous ADC word, a total of six words comprising a frame. In addition to the data, a clock signal and a frame synchronisation signal is sent to the surface electronics. The frame synchronisation signal indicates the beginning of the first word for the first ADC at a particular sampling time. The FPGA can also be configured to transmit test vectors (rather than measured data) to test the integrity of the communications link.

## **4.7 Surface Electronics**

This section details separately the following two purpose built cards for this project.

- VLDS Interface
- Multi-Purpose Interface

### **4.7.1 VLDS Interface**

The VLDS/IF is a 6U Eurocard printed circuit board that has been specially designed for this project to interface the VME bus to the VLDS recorder. It provides a path for sending commands to the VLDS and a means of both recording and reproducing data. An integral part is a daughter card that distributes signals from the front panel connector to the appropriate VLDS connector on the rear of the unit.

The VLDS/IF board is memory mapped into both VME and VSB address space. The VME address space is used by the host processor to send commands to the VLDS recorder. The VSB bus is used for the transfer of data from the VLDS to a data cache. This cache is dual-ported onto both the VME and the VSB buses to allow data to be streamed off the tape at high speed without interruption. Fig. 4.8 shows the printed circuit board layout for this card.

Sending commands to the VLDS involves writing them to a memory location mapped into VME A24:D16 memory space (base+offset 0x02). Groups of commands are written to this address in the same order that the VLDS accepts them (as described in the VLDS Operator Manual). A FIFO buffer on the interface card stores these commands in sequential order. It transfers them to the command interface on the VLDS, compensating for the relatively slow writing of commands to the recorder and de-coupling the host processor from the VLDS interface. A logic state machine implemented in a Xilinx FPGA provides the necessary handshake lines for writing these commands and for popping the FIFO buffer at the appropriate time. A maximum of 64 bytes can be stored and this easily accommodates the thirteen byte maximum length of a VLDS command. If commands are sent while the VLDS is busy with an operation they are ignored. As the VLDS command interface is bidirectional, the state machine also allows for the VLDS/IF reading status bytes from the VLDS across the same interface. Status data can be subsequently read from VLDS/IF by performing a read from the same VME A24:D16 memory location used for writing commands.

The VLDS/IF is tightly coupled to a specific dual ported memory card for VLDS data reproduction operations, it is used as a data cache. This card is manufactured by Chrislin Industries and is model CI-VME40 of 32 Mbyte capacity. Data is written across the VSB bus (via a 64 way ribbon connector). Once the reproduction is complete, the host processor can read the data across the VME bus. It is possible to interleave VSB writes and VME reads. However, this is avoided here due to the 'off-line' nature of the reproduction and the potential risk of data corruption (from interference with the DRAM refresh cycle due to host processor access and subsequent risk to data integrity). The 32 Mbytes of memory is filled in one reproduction operation.

Data is reproduced from the VLDS on two channels, each producing one byte for each data strobe at the data interface. This data is written across the VSB as four bytes per transaction. As such, a method of expanding the data width into four bytes is required. The design implemented uses four bi-directional FIFOs (each of one byte width) supplying data to the VSB. Each channel writes data into two FIFOs, in a fashion where the data path switches sequentially between each FIFO on a byte by



byte basis. This expands the data which is of a single byte width to be output as two bytes in width. Channel 1 data is written to address bits AD15-AD08 and AD31-AD24, commencing at the first byte and then switching between the two. Channel 2 data is written to address bits AD07-AD00 and AD23-AD16, in a similar manner. This obscure data format was used to simplify the printed circuit board layout. It was deemed easier to unscramble the data in software during the transcription process.

During data reproduction a logic state machine controls the data switching on the board and the VSB transactions, this is performed by a second Xilinx FPGA. Once the appropriate data reproduction strobes are received by the VLDS/IF the data is automatically input to the FIFOs in the appropriate order. As the FIFOs fill and exceed half their capacity (1024 bytes), a data write operation is commenced on the VSB. As there are only two circuit boards on the VSB there is no lengthy arbitration. The VSB transaction follows in a multiplexed fashion with the starting address being broadcast and data transferred in block transfers of 256 bytes. (The VSB addresses start with a zero offset from base address configured by jumpers on the board.) Refer to the appropriate document (IEC 821, 1986) for a description of the VSB transaction. These block transfers continue with the FPGA increasing its VSB starting address with each block transaction. When the VLDS reproduction is complete, the remaining data in the FIFOs is flushed into the memory card.

To record data onto the VLDS some other hardware is necessary. The VLDS/IF provides the path for issuing the record command, but it does not present data to the VLDS. All that is required is single or double byte wide data to be presented to the VLDS data bus and a recording data strobe of the appropriate timing. In this case the MPI card performs this function. Apart from joining the front panel connector to the daughter card, the ribbon cable also needs to be connected to the additional hardware. Note that the memory card is not required for data recording, nor is the VSB connection.

The VLDS/IF has a status register mapped into VME A24:D16 memory space (base location). It is possible to monitor whether the VLDS is selected (active low on bit0) or whether it is busy with an operation (active low on bit 1) with a read from this location that is memory mapped as an 16bit port.

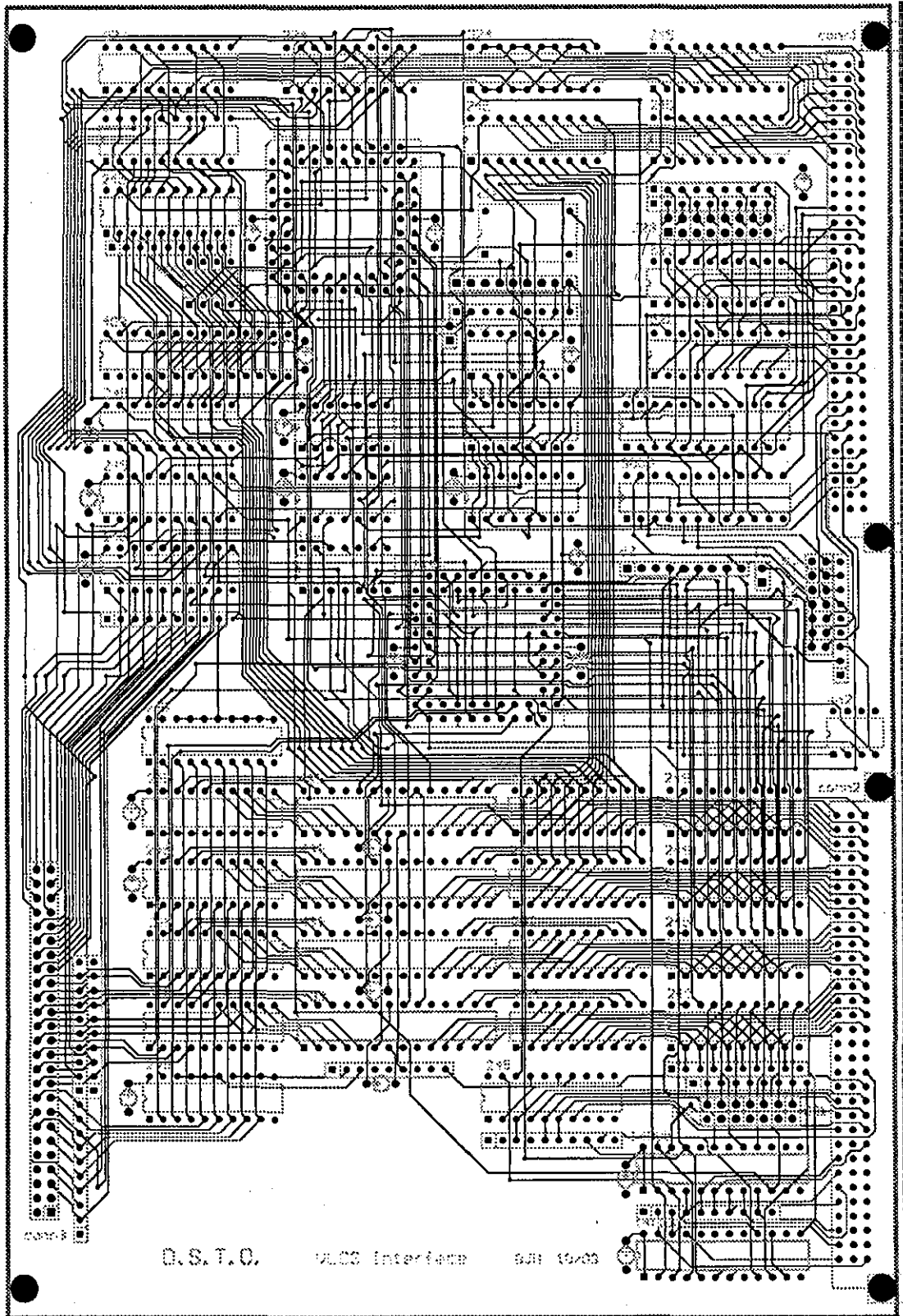


Figure 4.8 VLDS/IF Circuit Card

## 4.7.2 Multi-Purpose Interface

The MPI is also a 6U Eurocard and it synchronises much of the activity during data collection. It performs numerous functions, including generating the acoustic waveforms, synchronising their transmission and acting as a data interface between the serial link from the towfish and the VLDS. As it is intended only for this experiment the card remains as a wire-wrap board.

During data recording the host processor is a slave to the MPI board. It is mapped into VME A24:D16 memory space of the host processor. After setting the trigger enable bit in the MPI status register (active high on bit 0) the processor polls this same register continuously (reading from the base address). It either detects a completed pulse transmission (active high on bit 0) or a termination of the recording (active high on bit1). On detecting a complete transmission it loads the FIFO buffers (with subsequent writes to the base address+offset 0x04) with a maximum of 2048 words of 12 bits, representing the next transmission pulse (the most significant four bits are not used). Flushing of the FIFO and subsequent generation of the transmit pulse occurs after a trigger is received from a function generator. In this manner an accurate pulse repetition frequency can be conveniently set on the front panel of a function generator. This repetition rate is more accurate than would be possible using the timers on the host processor.

The transmit waveforms can range in time duration up to 16ms. This is a combination of the rate at which the FIFO is flushed into the D/A converters and the number of discrete values loaded. Once triggered, the digital waveform values are clocked at the selected rate until the FIFO is empty. The rate ranges from 125kHz to 16MHz and is set with three DIP switches. Each digital waveform value comprises a 12 bit word, corresponding to one of 4096 different analogue output levels. A separate connection to the power amplifier disables the output for all but the 16ms during a transmission, this reduces amplifier noise during echo reception. The output analogue signal is also low pass filtered to remove any higher frequency components from the transmission.

Acoustic data is received from the tow fish in a serial format. In addition to the data (that is clocked at 16MHz), both a clock signal and a frame synchronisation pulse are received. The synchronisation pulse indicates the beginning of a new sampling frame and the data following this comprises sensor one through to six in order of high byte followed by low. A total of 48 bytes are transmitted in each frame, representing four sampling points on all six channels. A Xilinx FPGA converts the serial stream into byte wide data. It inserts a motion synchronisation byte before clocking the data into a FIFO for writing to Channel 1 of the VLDS. As the data rate is slightly lower than the 2Mbytes/sec that is required by the VLDS, padding data is inserted in blocks into the data stream. Channel 2 of the VLDS is used to flag the data padding. Data on the towfish side of the FIFO is synchronised to the clock signal generated by the underwater electronics. As the VLDS requires a phase stable clock signal, data on the VLDS side of the FIFO is synchronised to a different clock signal. The FIFO buffer provides a mechanism of translation to a stable clock source.

Motion synchronisation data is received from the PC in a parallel format. The PC outputs a count of 256 possible values and increments every fifty motion data packets; this corresponds to twice a second. This byte of data is held in a register on the MPI until the FPGA signals it to be output to the VLDS data stream. Only the lower four bits of this byte are used, with the upper four bits being used to flag the presence of invalid data.

In writing data to the VLDS each frame consists of forty-nine bytes. The data packets are continually written to the FIFO and if a record operation is not in progress the FIFO is reset at the end of each. On receiving a signal that the recorder is ready for recording, the data strobos commence and data is output from the FIFO. The data strobos continue until the record operation ceases. Note that the final data packet will be corrupted as the VLDS records data on 64 kbyte boundaries and this is not divisible by the number of bytes per packet.

## 4.8 Data Reproduction

After data is collected in the field the equipment is brought back to the laboratory for transcription. In the field the videotape media is used, but for post processing a more accessible media is desired. The VLDS is ideal for collecting data, but its non-standard media format makes it less convenient for data analysis.

Transcription of data is performed on a different VME chassis to that for data collection. This chassis is connected to an IBM Risc workstation via a Bit3 VME to Micro Channel converter. This converter acts like the host processor in the field measurements. It becomes master of the VME bus and sends commands to the VLDS/IF board. It also retrieves data from the dual-ported memory card.

VLDS data is reproduced in blocks of multiples of 64 kbytes from a given block number. It is transferred via the VLDS/IF interface to the Chislin memory board mapped into both VME and VSB memory space. The data flow is such that it enters the memory board on the VSB bus and is read by the converter out on the VME bus. This memory card is of 32 Mbytes capacity, which corresponds to a maximum of 512 VLDS data blocks in each access.

Data stored in the memory card is transferred to the workstation in blocks of maximum size 16 Mbytes, this is a restriction placed by the Bit3 converter. As such, two block data transfers across the converter card are necessary to transfer the 32 Mbytes of data from each VLDS reproduction. Within the workstation files of any convenient size can be written and backed-up onto a 4mm DAT tape drive.

Motion data from the PC is also transferred onto a workstation for subsequent analysis. As this data requires calibration it is not merged with the acoustic data at this stage.

## 4.9 Software

Software for this project is written in the C language and falls into a number of categories. Data collection software executes on the VME processor under the OS/9 operating system. Motion data collection software is on a PC in a DOS environment. Data reproduction software is written for an IBM Risc workstation and the AIX/Unix operating system. For both calibration and processing of all data sets (motion and acoustic) a Unix workstation is used, this is a PC workstation running Linux.

### 4.9.1 Motion Data Collection Software

The software for collecting motion data runs on a PC. Its function is to create files from data it has read on a serial port. In addition to this, it also creates a synchronisation word that is output on its parallel port. Due to the reasonably high data rates involved with the recording, this program consumes all resources of the PC when executing.

The recording routines create a new file when invoked. Before writing data to this file a search is made for the block marker associated with the start of the data from the serial port. As the incoming data is a continuous stream this marker must be found as a point of reference before recording can commence. After this, the data stream is read in a block fashion and written to disk at the same time. This process continues until it is interrupted by a signal from the keyboard.

### 4.9.2 Motion Data Calibration Software

The motion data is in a raw format and must be calibrated into standard units for subsequent processing. The translations are to be calibrated into units of  $ms^{-2}$ , while the rotations are calibrated into units of  $^{\circ}s^{-1}$  of rotation. Both types of transducers must be calibrated for gain and offset from reference measurements.

The motion calibration takes the raw data collected in the field and transforms it with the appropriate scaling and offset to a value expressed as a standard quantity. Each of the 6DOF transducers have been measured for performance on standard calibrating devices. For example, the gyros are placed on rotating platforms with selectable speeds. The performance of the transducers are measured at different speeds and their response compared with the expected. From this comparison a gain and offset value is determined for each. These calibration factors are applied to the raw data, after which the processed results are written to another file for later reference.

### **4.9.3 Acoustic Data Collection Software**

The software for the acoustic data collection is relatively simple as many of the operations of the system are hardwired. When a session commences the length of the recording is requested, as is the type of transmit pulse (or pulses) required. From the characteristics of this pulse the discrete points of the waveform are calculated and stored in memory. The host processor loads the first waveform into the MPI waveform FIFO and issues a command to the VLDS/IF for the VLDS to commence recording (the command implemented is for a finite number of data blocks to be recorded). Subsequent to this the host sets the appropriate bit in the status register (bit 0) of the MPI to allow triggering of the transmit pulses. The host then remains in a loop, checking the MPI status register (by continual polling) for either a termination condition (active high on bit 1) or a waveform load (active high on bit0). The VLDS will take several seconds to start recording and it is not possible to determine the stage of the cycle that the actual recording commences.

In addition to the recording commands, other commands are required for tape handling operations. These commands are performed outside the data recording loop and involve such things as rewinding the tape, ejecting it and checking the VLDS status registers.

#### **4.9.4 Acoustic Data Transcription Software**

The transcription program retrieves data from the VLDS via the Chrislin memory board in a VME chassis. Again tape control operations have to be included for control of the tape transport. The main routine prompts for a starting block number, a finishing block number (that must be no more than 512 blocks apart) and a filename for transfer. The data is extracted off the tape in blocks of 16Mbyte until the entire set has been transferred. After each block is extracted it is transferred to the workstation and written to the nominated file. These files are subsequently written to a 4mm DAT tape drive.

#### **4.9.5 Acoustic Data Calibration Software**

The acoustic data consists of blocks of valid data interleaved with data padding. The padding must be removed from the sequence prior to data processing. To remove the padding the flags on odd bytes in the file must be interpreted and only valid data written to an intermediate file. The acoustic data of this intermediate file has each sensor reading represented as two bytes. This data is raw and must be calibrated for the particular receiver and expressed in standard units of dB re 1V/ $\mu$ Pa. Each receiver has a different response and this must be calibrated for final processing.

#### **4.9.6 Analysis Software**

The different processing algorithms shall be detailed in the next chapter describing the data analysis.



## **Chapter 5      Results from Synthetic Aperture Sonar**

### **5.1    Introduction**

Field trials of the experimental sonar included both test tank measurements and those in the ocean. The test tank experiments provided an integrity check of the acoustic components prior to the ocean field trials. They also allowed a calibration of the system under controlled conditions. The ocean experiments were performed a number of times in various conditions and the data was used in the generation of real aperture and synthetic aperture sonar images.

The test tank experiments were performed without the motion transducer section of the towfish. Acoustic data was collected from the echo returns of a number of test targets suspended in the tank. To emulate the normal along track motion of the sensors the array was moved vertically in the tank. With the targets suspended vertically this was equivalent to point targets in the azimuth of the sonar in a normal tow configuration. Data was recorded at discrete positions as the array was lowered past the targets. This data was processed at a later stage to create images of the targets.

The field trials were performed with both the acoustic sensors and the motion transducer equipment assembled together as a complete sonar system. The underwater platform was towed behind a surface vessel and data collected from a number of locations. The sites were chosen to be representative of the wide range of sea floor types. These included those with few underwater features and others with a considerable number. Calibration measurements were also performed with test targets of known geometry and target strength placed on a featureless sea floor.

## **5.2 Sonar Test Tank Measurements**

### **5.2.1 Introduction**

The experimental data recorded in the test tank provided the opportunity to generate sonar images of known targets with minimal disturbance from external influences. Both acoustic noise and platform motion were brought to minimal disturbing levels in the tank. The test tank was also valuable for verification of the performance of the sonar. Although the constituent acoustic components had been tested individually it was not until the tank experiments that the entire acoustic section of the sonar operated as a complete unit.

Test tanks of large dimension are not common. It was fortunate that such a tank was available in Sydney for this experimentation. The test tank was part of a test facility for the production of low frequency hydrophones for the military. Low frequency hydrophone testing requires a tank of considerable size to reduce near field effects. The tank was also particularly quiet and relatively free of interfering noise sources (despite being several hundred metres from a metropolitan train route). The tank was located at the Sonar Test Facility on the premises of GEC Marconi in the suburbs of Sydney, Australia. The Sonar Test Facility consisted of the tank and numerous pieces of computer equipment to control the underwater platforms. Also present at the facility were other associated equipment such as reference hydrophones for calibration purposes.

The Sonar Test Facility test tank was of cylindrical construction with walls of redwood joists. Redwood walls are particularly suitable for sonar testing applications as they absorb acoustic energy better than many other structural materials. The joists were braced by high tensile steel bands at regular intervals down the tank. It rested on pneumatic springs and these provided isolation from external acoustic noise sources. The tank was approximately 7.5m in diameter and 8.7m in depth. At one end was a movable platform that could be rotated in azimuth. This azimuth rotation was computer controlled and could be stepped to desired angles with a high degree of accuracy. The platform could also be lowered to any elevation down to the bottom of the tank. Raising of the platform was under manual control with an electric motor.

providing the lift. Unfortunately, the poor motor control made it difficult to obtain good accuracy in elevation during the data collection.

### **5.2.2 Test Tank Experiments**

The test tank experiments involved collecting data of acoustic returns from test targets at regular and equally spaced elevations in the test tank. The test targets were suspended vertically at a constant depth and distance from the path of the array as it was lowered in the tank. The acoustic data recorded at each elevation was stored as separate data sets for subsequent processing. An individual data set was a continuous recording of the acoustic returns for a number of sequential transmissions in the tank. The same acoustic transmissions were repeated at each depth and consisted of a number of different narrowband and broadband signals, each varying in duration and frequency.

The geometry of the experiment in the test tank is depicted in Fig. 5.1. The test targets were suspended on the same cable at a distance of 4.5m from the closest pass of the towbody. The towbody was lowered into the tank and the first data collection started at an elevation of 3.8m below the top of the tank. Data was collected at 5cm intervals to a depth of 8m, with the depth being marked by graduations on the supporting structure. A total of 80 separate measurements were made. At each depth the towbody was left to settle for a short time so lateral motion of the structure could be damped by the tail fin assembly in the water.

There were two types of test targets used in the experimentation. One was an air filled plastic sphere of about 5cm in diameter. The other was a Freon filled aluminium sphere of about 10cm in diameter. The aluminium spheres were specially constructed to be of high target strength to incident acoustic energy. They are designed to focus incident energy back to the source. At a frequency of 100kHz they have a target strength of -11dB. A total of five test targets were arranged on a cable, an aluminium target followed by two plastic, followed by another aluminium and finally a further plastic target. They were separated by distances greater than 12cm to have a total distance of 1.3m from first to last.

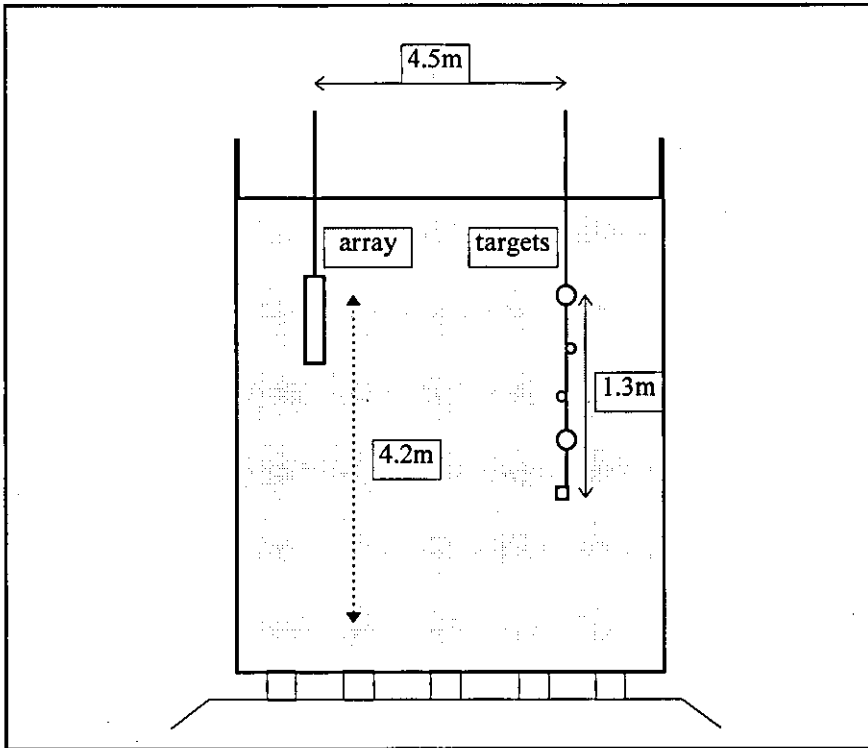
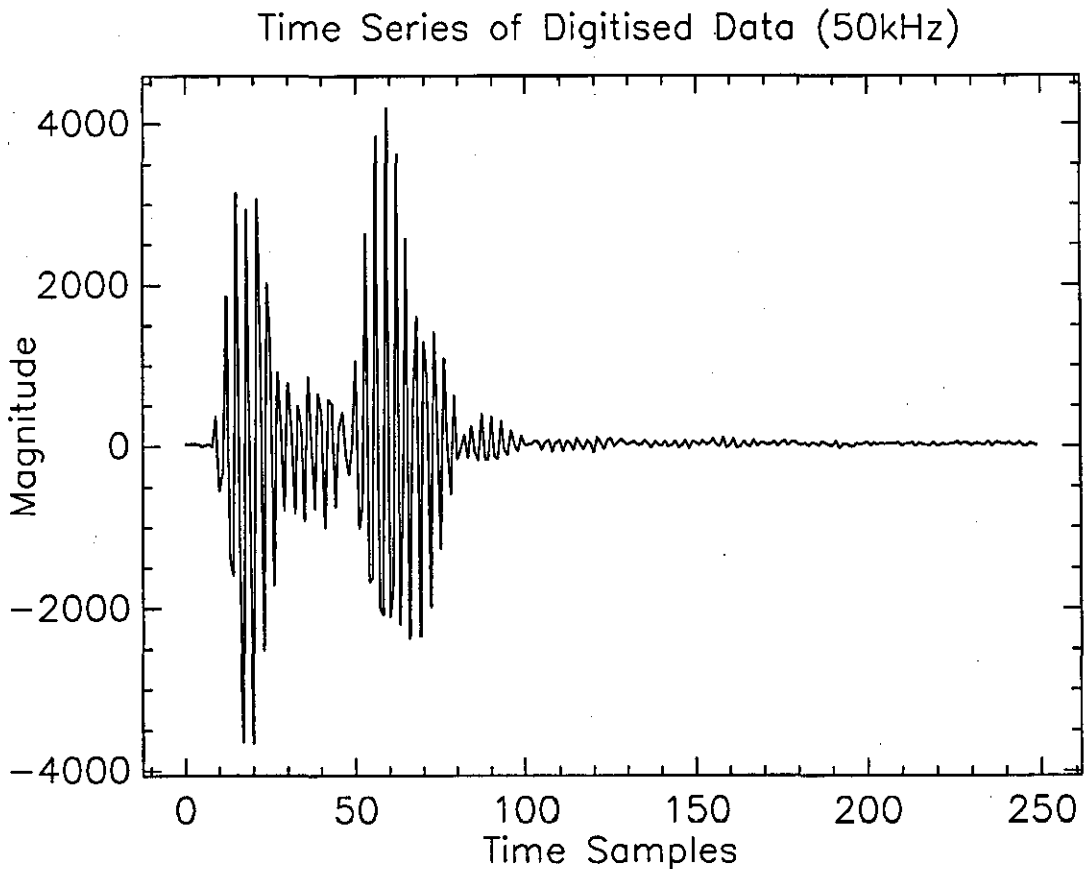


Figure 5.1 Geometry of Tank Experiments

The acoustic transmissions in the tank consisted of both narrowband and broadband signals. The narrowband signals were Hanning weighted pulses of several cycles with centre frequencies of 50kHz, 55kHz, 60kHz, 65kHz, 70kHz, 75kHz and 80kHz. The broadband transmissions consisted of chirps of approximately 80 cycles. The four chirps were over the frequency ranges 50kHz to 80kHz, 80kHz to 50kHz, 60kHz to 70kHz and 70kHz to 60kHz. Each transmission was separated in time by an 83ms interval, with the narrowband set being followed by the broadband in a repetitive order. The time interval between transmissions was sufficient for reflections from the previous to be reduced to a negligible level. The cycling of the transmissions was repeated until about 60 seconds of data was collected.

### 5.2.3 Test Tank Data

The recorded data was transcribed off the VLDS cassette and copied onto DAT media after the experimentation was complete. This was performed at the laboratory in the manner as described in Chapter 4. Each data set for different elevations comprised a raw file of around 130 Mbytes that was transcribed. Due to the large and unwieldy size of the files they could not all be stored on the processing computer at one time. The data sets had to be pre-processed to remove only a fraction of the original data (for example, a number of transmissions of a particular frequency) and these were written to smaller files. They could then be combined to create images over the entire aperture in the tank.



**Fig.5.2** Transmit Pulse at 50kHz

The pre-processing of the raw data files involved a number of steps. The data from each sensor was extracted and all data padding (introduced during recording due to recording timing differences) removed. Once extracted a single input channel was

searched for the location of particular transmit signals to synchronise the data extraction. These signals consisted of the transmit pulse cross-talk and were of particularly high amplitude due to cross-coupling between the transmit array and the receive array. They could also be identified by the acoustic reflections that propagated down the tow body. The time series of a single 50kHz transmit pulse is displayed in Fig. 5.2, the first pulse is the electrical cross-talk and the second is the acoustic reflection along the towbody. Once the 50kHz pulse was located (using a frequency domain search algorithm to align the data on the envelope of the transmit pulses) the location of any transmission in the sequence could be determined from the time delay between transmissions.

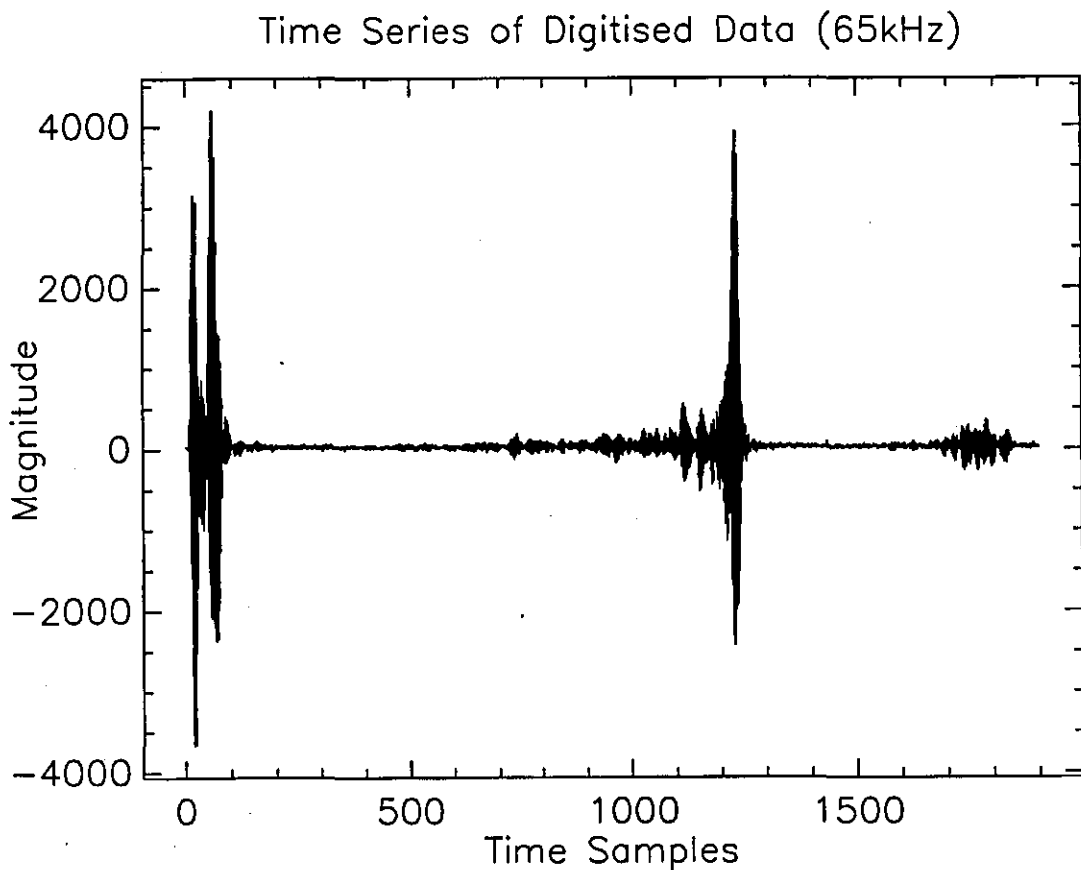


**Figure 5.3** Single Acoustic Return at 65kHz

Transmissions of the same frequency (or frequency sweeps) were extracted from the raw data files and placed in separate files for post processing. For each transmission a total of two thousand data points were extracted. This was sufficient data to identify the transmit pulse, the first return from the targets and the first reflection from the rear of the test tank. An example of an acoustic return is shown in Fig. 5.3, this is a 65kHz

transmission. The very low background noise level in the test tank is apparent from the good quality of the received signal.

#### 5.2.4 Simulations

The broadband beam pattern generated by the experimental synthetic aperture sonar is simulated in this section. The side lobe suppression with broadband signals is of particular interest as the mix of frequencies acts to reduce the peak side lobe levels by smearing them across a range of azimuth angles.

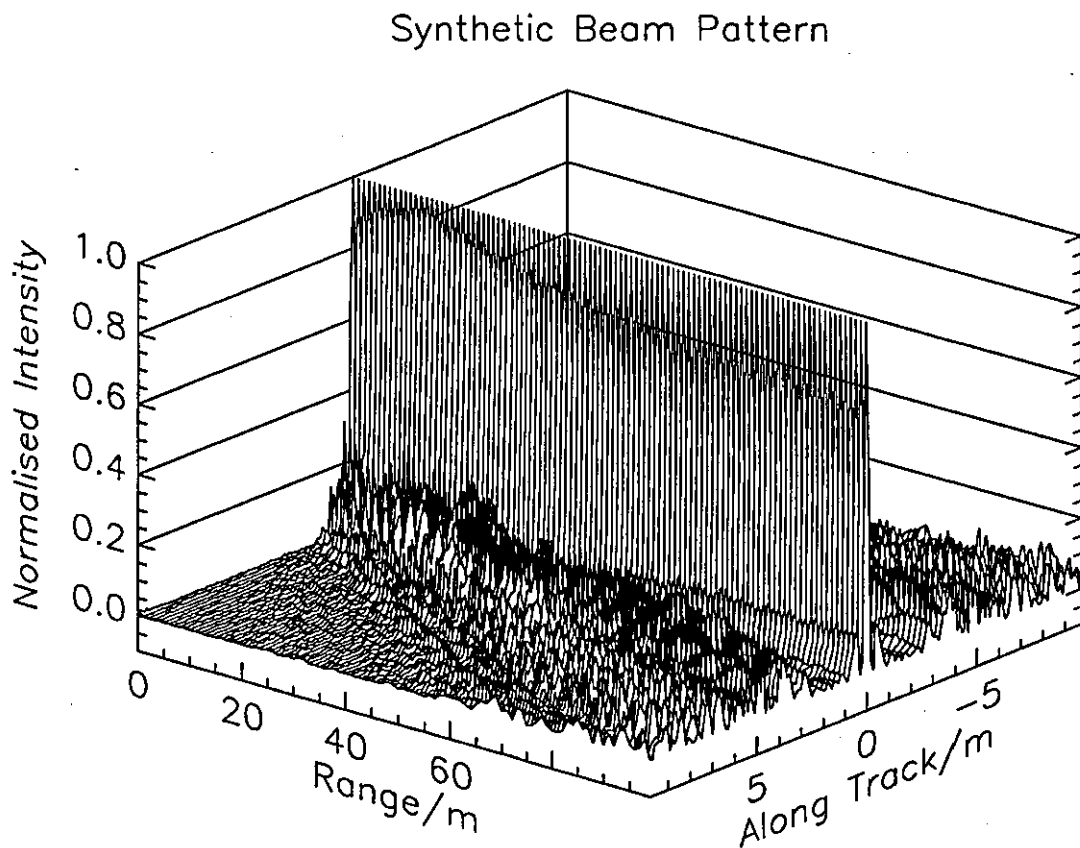


**Figure 5.4** Synthetic Aperture Beam Pattern

The simulated beam pattern broadside to the synthetic aperture is displayed in Fig. 5.4. The range is considerably greater than that measured in the test tank. This beam pattern was created from narrowband transmissions of a single acoustic element, with a different frequency at each synthetic array position. Note that the main lobe of the

beam pattern remains a constant width as range increases. The effect of the broadband signals is evident in the smearing of the sidelobe response at azimuth angles away from the main beam. No account has been made for non-ideal platform trajectory or any uncertainty in the aperture sampling locations. Also, only simple 'line of sight' propagation is considered with no complex acoustic interactions.

### **5.2.5 Real Image Processing**

The real image processing of the test tank data involved combining a number of receive element responses into a single response through beamforming in the broadside direction to the array. From these single responses three-dimensional images of the targets were created.

The data processing to produce the final target image involved a number of steps. As the receive signals were not noisy and of relatively good quality it was not necessary to filter the individual element responses. Consideration was made for the variation in response between elements of the real array aperture and each was normalised to be equivalent. Spatial response tapering was applied at the ends of the array to reduce sidelobe levels in the beamforming, with a Hanning spatial function determining the tapering of each element. The beamforming was performed in the time domain and involved a simple coherent addition of the tapered response of the individual acoustic elements. At each elevation in the tank the same elements of the array were beamformed and the envelopes of all were combined to produce a three dimensional topological representation of target response as a function of range and azimuth. No consideration was made for the variation in time alignment of the beam responses between elevations and a worst case variation of a single sample period was possible; thus any degradation decreased with frequency.

The result of real aperture processing for a three element array is displayed in Fig. 5.5. The intensity of the beamformed response is plotted in uncalibrated units. The signals consisted of several cycles at a centre frequency of 50kHz and the target image is plotted over a 3m distance in elevation and slightly over 1m in range. The target strength image displays a number of strong peaks that correspond with the high target



strength aluminum targets. However, the image is rather noisy and the smaller targets are not easily resolvable in this clutter. A peak in the response exists at the 0m elevation level and this corresponds to a surface return from the top of the tank. The wide beam response with only three elements in the array is likely to be the reason that the smaller targets were not resolved.

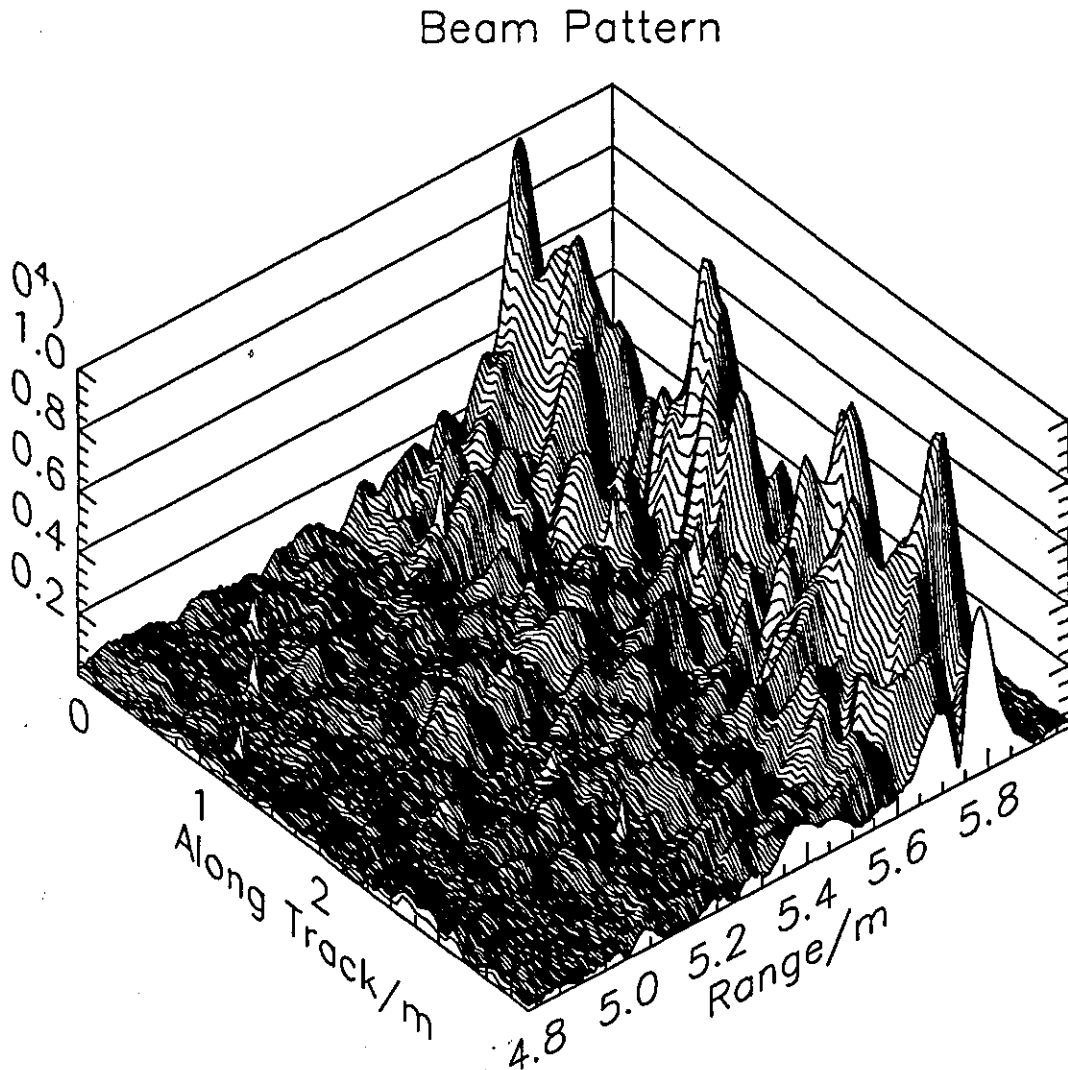


Figure 5.5 Real Processed Image at 50kHz

### 5.2.6 Synthetic Image Processing

The synthetic image processing of the test tank data involved a greater amount of data computation than the real image processing. Synthetic images are produced for both a single element traversing the synthetic aperture and for a three element array doing the same.

## Beam Pattern

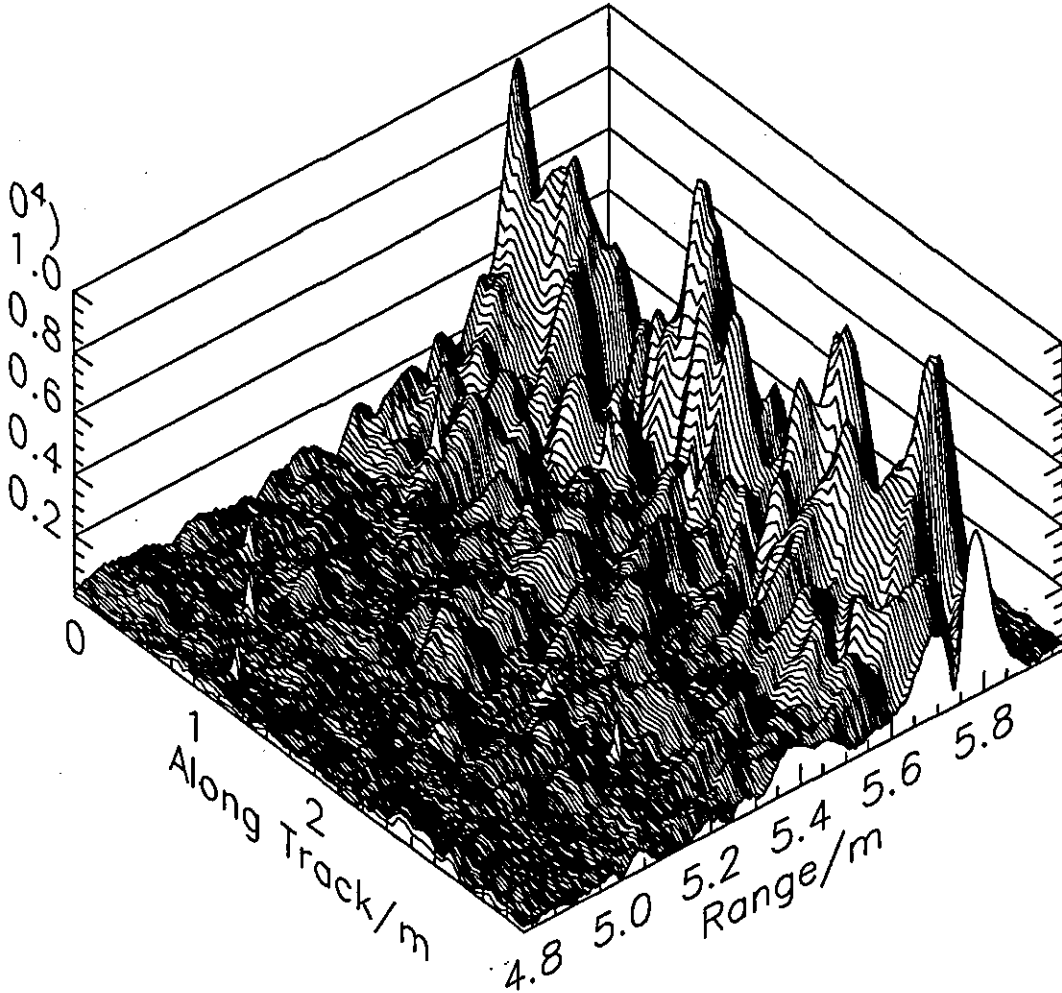
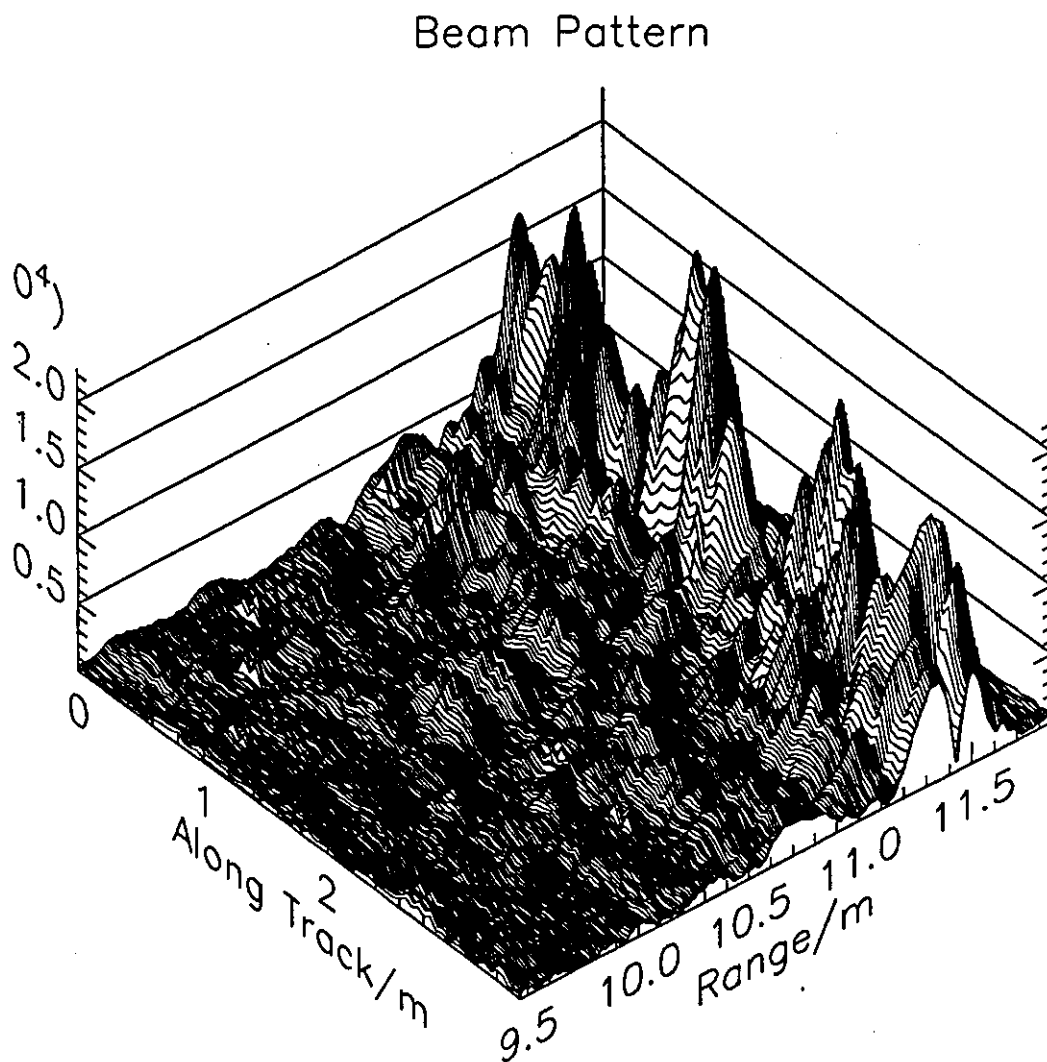


Fig. 5.6 Synthetic Image at 50kHz with One Receive Element

The difference in absolute time reference between pings from the continuous recording was of greater importance in the synthetic array processing than with the real image processing. One receive waveform was the timing reference and all other received waveforms that comprised the synthetic array were time aligned to it. Where the time difference was less than a sampling duration the adjacent points were interpolated to a response between the two adjacent points.

The synthetic image of a single element at 50kHz is displayed in Fig. 5.6. The synthetic array was of length seven elevation positions. The received waveforms from each elevation position were coherently combined to form the response at the mid-

point of the array. To produce an image the waveforms were envelope processed and placed beside each other in the three-dimensional representation shown. Although the two peaks of the aluminium test targets are visible, they are not well resolved. The azimuth size of the targets are greater than expected.



**Fig. 5.7** Synthetic Aperture Image at 50kHz with Three Receive Elements

To investigate the unexpected features of the test tank synthetic aperture image another image is shown in Fig. 5.7 for the same 50kHz centre frequency (note that the range values are inadvertently double the actual). Two differences in the processing exist here. Firstly, the length of the synthetic aperture was increased to eleven elevation positions in an attempt to improve the azimuth resolution of the targets. Secondly, the response at each elevation was the real beamformed response of three receive sub-arrays. This real aperture beamforming reduces the element beamwidth at

each synthetic aperture position. However, despite these two changes the azimuth resolution of the targets did not improve as would be expected.

The synthetic aperture images did not display an expected sharp azimuth resolution. The most likely explanation for this is that the array was not completely stationary in the water when data was collected at the different elevations in the tank. Therefore, the assumption of the transmit pulses remaining at the same time position between subsequent pings was not correct. Evidence for this can be found in the degradation of the azimuth resolution as the synthetic aperture is increased, this is contrary to what is expected of a synthetic aperture.

### **5.2.7 Conclusions From Test Tank Measurements**

The test tank measurements verified that the acoustic sections of the sonar operated as expected. Large test targets could be distinguished with both the real and the synthetic image processing.

The synthetic image processing indicated some residual and unexpected transducer motion during the tank test experiments. The test targets were not as well defined as would be expected and a plausible explanation for this is motion of the array. This explanation is not unreasonable as the array was suspended by a long pole and lateral motions were not completely constrained. Perhaps insufficient time elapsed between re-positioning the array and the data being collected at each position. Unfortunately the experiment could not be repeated due to limited access to the test tank.

## **5.3 Motion Measurements**

### **5.3.1 Introduction**

The motion data is used in the estimation of the spatial location of the sonar. This requires processing of the three translation and three rotation measurements collected by the motion measuring package. This data was collected each time the sonar was trialed in the sea. As such, a number of data sets were collected and analysed for this section.

The motion data is examined in isolation from the acoustic data. The characteristics of the data as a time series and the spectral components are discussed. The raw data has to be processed to produce relative displacements (translation and rotation) of the tow fish between consecutive sampling points. The translation sensor data is doubly integrated to produce displacement measurements, while the rotation data is also integrated to give the rotational displacement.

### **5.3.2 Motion Experiments**

The experiments were conducted on a number of occasions in the confines of Sydney Harbour. The motion measuring section was always operational during these trials. On the occasions when the acoustics section was not present the motion package was a useful tool to verify the stability of the underwater platform. The towfish was towed behind a surface vessel and the data was collected on the logging PC as described in Chapter 4. The locations were in shallow water to a maximum depth of 30m. The towing position on the surface vessel restricted the operation to relatively fine conditions within a small range of sea states.

### **5.3.3 Motion Data Processing**

The motion data was transcribed from the logging PC after returning to the laboratory. As the data was in a raw format it had to be calibrated before subsequent processing. The calibration applied known gains and offsets to the measured data. Once calibrated

the processing algorithms could be applied. The angular velocity measurements were integrated to angular displacement and the linear acceleration measurements were doubly integrated to produce a position measurement.

The translation acceleration data collected in the vertical direction gave the heave motion of the towfish. This data could be correlated with the depth sensor as an independent check of the acceleration data. The depth sensor was not particularly accurate, but the trends in the data could be used to verify the processing of the acceleration sensor data and demonstrate any limitations of the technique for motion sensing. The raw acceleration data, the integrated displacement and the depth sensor data are displayed in Fig. 5.8. In these graphs the time interval is the same for all three.

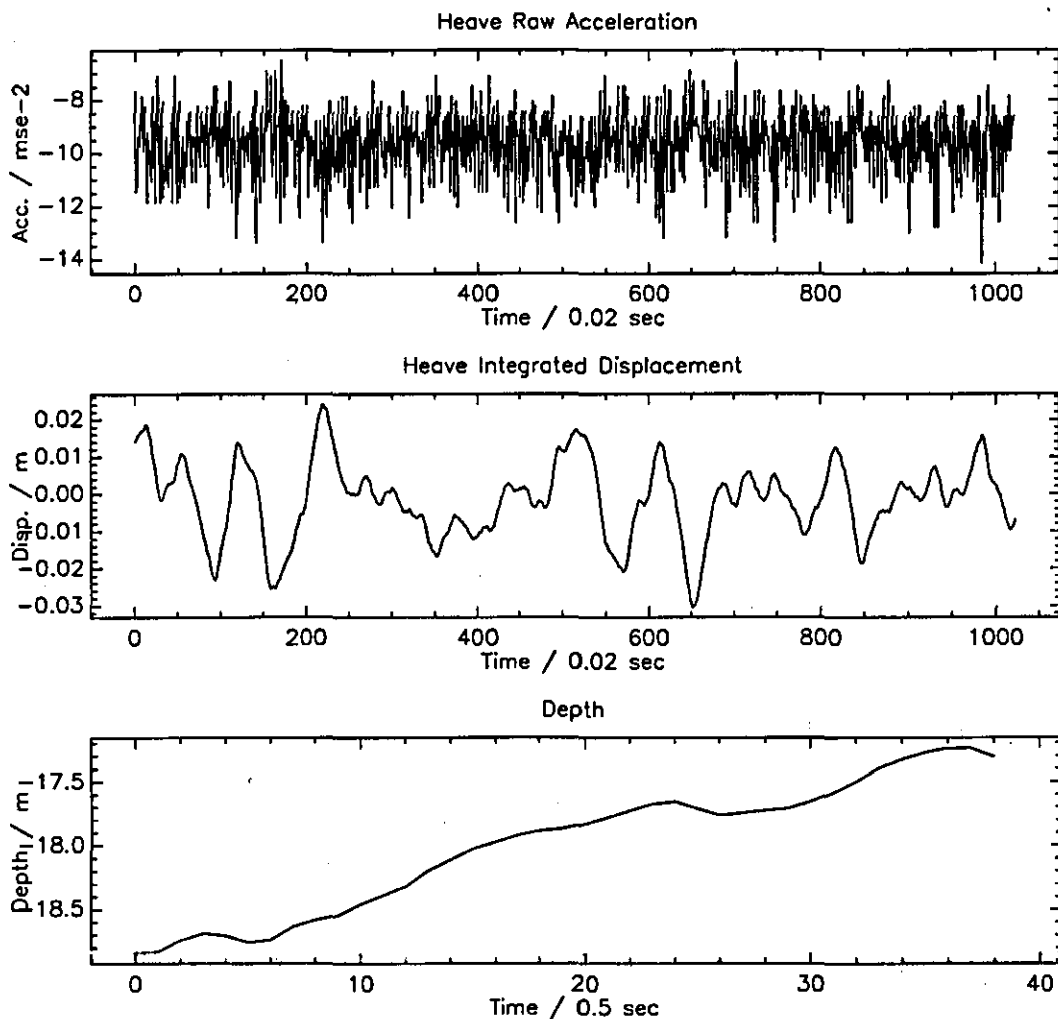


Fig. 5.8 Heave Motion and Depth as a Time Series

The first general observation of the calculated heave displacement is that the motion is of much smaller amplitude (5cm) than the variation in the measured depth (1m). The calculated motion also exhibits higher frequency components than the depth data, this is substantially due to the limited bandwidth of the pressure transducer. The depth data exhibits a very low frequency component that is not evident in the calculated motion.

The general observations of the calculated heave motion demonstrate some genuine limitations associated with the use of acceleration sensors to determine towfish trajectory. Such sensor data must be doubly integrated and this reduces the signal-to-noise level for decreasing signal frequency. The data here exhibited this problem as the low frequency motions were not resolved. Low noise and very accurate motion sensors would be required to reduce this problem. Although the effect of heave motion is not as significant as sway, the same low frequency drifts would also be present in the actual sway motion and not resolved with the motion transducers.

The depth variation demonstrates the relatively large motions experienced by a towbody in shallow water. Without long lengths of cable acting to dampen the tow vessel motion the towbody diverges from the ideal trajectory considerably. Over a period of ten seconds the depth of the towbody varied by more than 1m. At a height of around 10m above the sea floor the depth variation would have a considerable impact on the resulting image. Such motions can not easily be measured and result in significant degradation of the sonar image.

The roll rotation motion is displayed as a time series and a relative power spectrum in Fig. 5.9. Roll does not have a significant impact on a synthetic aperture image as beam patterns are normally wide in the elevation plane. The interest in this data is the poor tow configuration revealed during the trials. A large peak in the power spectrum appears at around 12 Hz. This peak is the result of cable 'strumming' during the trials. Two cables were required to provide sufficient electrical conductors for both the acoustic sensors and the motion measuring equipment. However, these two cables could not be sufficiently well bound together and even a flared jacket around the cables could not prevent the oscillation. The oscillation was exacerbated by the need for a depressor on the towbody to ensure it flew at a sufficient depth during the

experiments. This cable oscillation demonstrates the requirement for a well designed and balanced tow body to minimise the amount of variation in trajectory and any other unwanted motion.

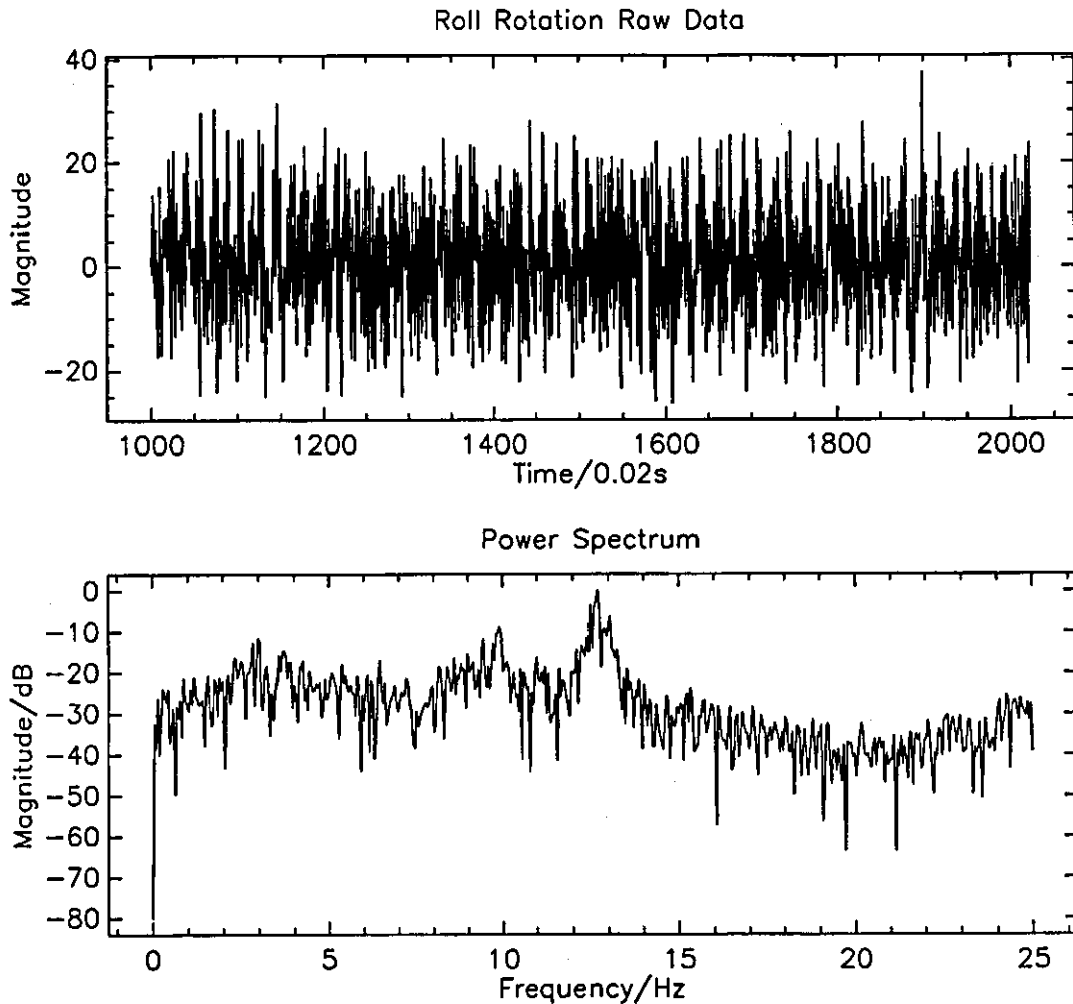


Fig. 5.9 Roll Motion as a Time Series and Power Spectrum

The calibrated sway data and the resulting calculated displacement is displayed in Fig. 5.10. Sway motion degrades the synthetic aperture more than any other motion. In the other directions only a component of the motion degrades the aperture, however, in the sway direction the full motion has a degrading effect. The sway motion is cyclic and perhaps the strumming of the tow cable has resulted in this. The maximum amplitude of the calculated motion is 2cm, more than a wavelength at the maximum operating frequency of 80kHz. Clearly this would cause degradation of the sonar image. The motion is of sufficiently high a frequency that the length of the aperture would have to be reduced to only a short interval to reduce the degrading effects. The



effect of the motion is reduced as the frequency is lowered and the wavelength increases.

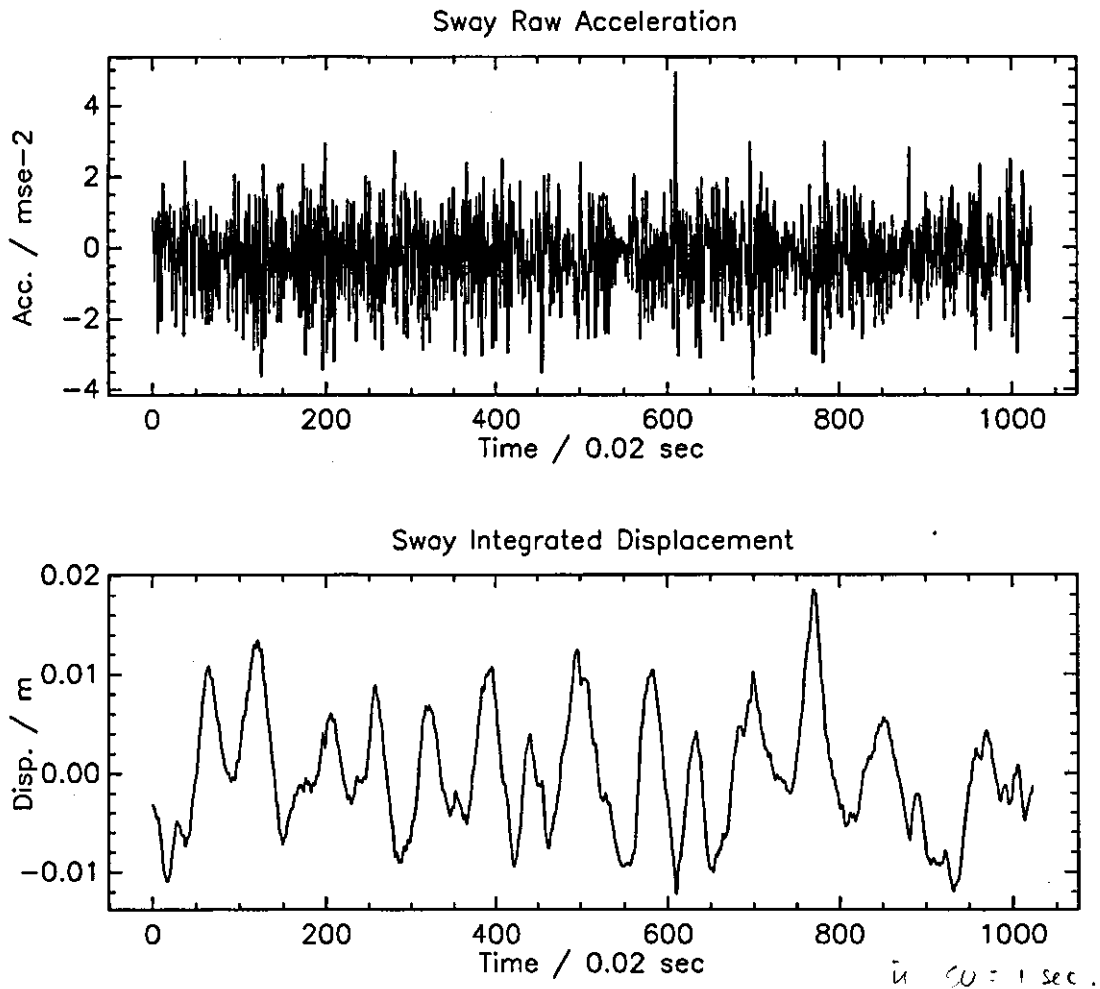


Fig. 5.10 Sway Motion as a Time Series

### 5.3.4 Conclusions From Motion Data

The limitations associated with the use of motion sensors to measure deviation in platform trajectory has been demonstrated in this section. The greatest limitation for acceleration transducers is their inability to resolve low frequency motions after integration to displacement.

The influence of sonar tow configurations are also evident from the motion measurements. It is apparent that shallow water synthetic aperture imaging would be much more prone to the degrading effects of platform motion.

## **5.4 Sonar Measurements**

### **5.4.1 Introduction**

The field trials were the culmination of the research activity into the synthetic aperture sonar. They were performed on numerous occasions in Sydney Harbour over a period of about two weeks.

The data produced from the field trials was intended to demonstrate the principles of the synthetic aperture processing techniques when combined with motion data from the motion measurement package.

### **5.4.2 Experiments**

The experimental data collection was performed at a number of locations in Sydney Harbour. The sites were chosen to represent a range of sea floor types that could typically be encountered. At some of these sites a number of test targets were placed on the sea floor. As these targets were of known dimension and target strength they were intended to produce a calibrated response. The targets were approximately placed at between 5m and 15m from the path that the sonar would take when towed behind the vessel.

### **5.4.3 Processing of Field Data**

It became apparent that the data recorded during the field experiments had severe corruption. It was noticed that the electronic circuitry that resided in the underwater cannister was suffering from severe corrosion due to the environment in the cannister. As such, most of the analogue to digital converters were not functioning correctly. The data was saturating at negative values less than full-scale as displayed in Fig.5.11.

It was not possible to correct the data values as the negative offsets varied and were not deterministic. Only one sensor produced reliable data during the experimentation.

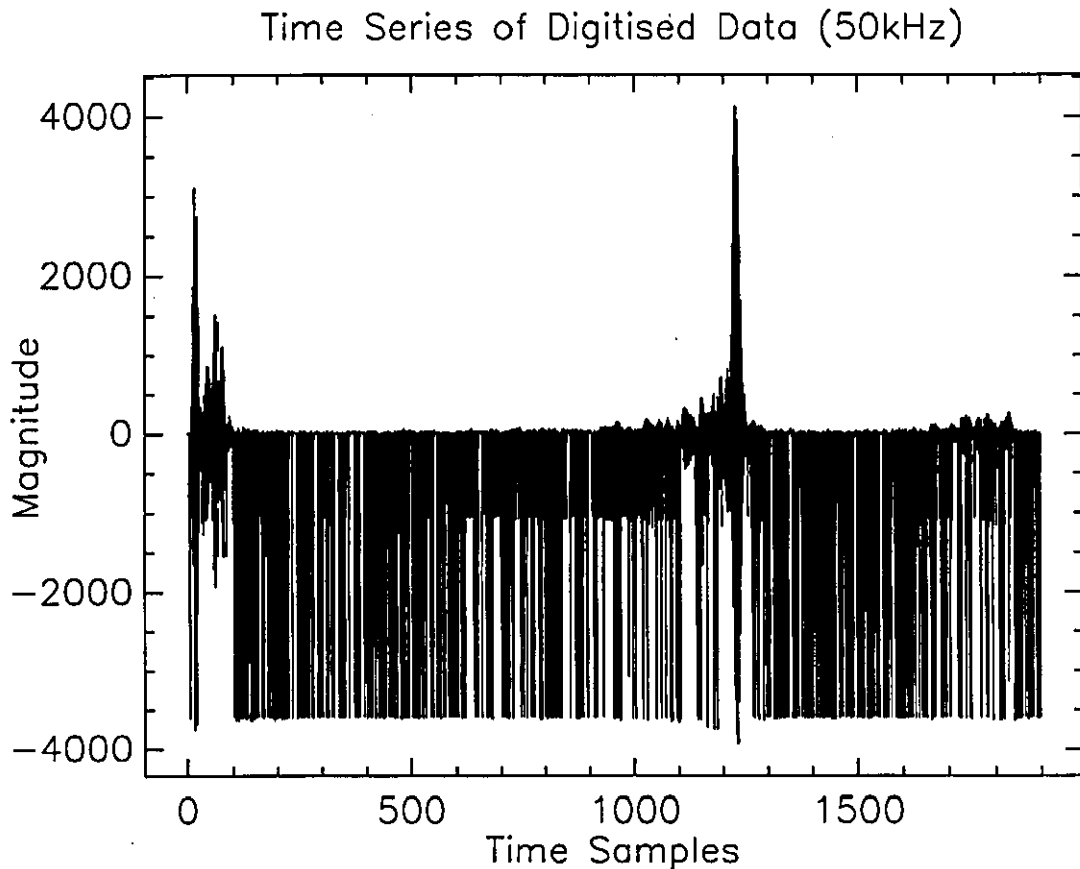


**Fig.5.11** Corrupted Data Sample at 50kHz

As the experimental data was not of sufficient quality for producing synthetic aperture images a number of waterfall plots were produced of the envelope response of a single element. In this representation the envelope of a single element is plotted on a logarithmic scale for subsequent pings. Each ping is consecutive with time increasing down the graph. Such representations are useful in identifying data sets that would benefit from synthetic aperture processing. A strong target will be visible in a number of the responses and it will appear to move in a parabolic fashion with range across the waterfall.

The first waterfall image is displayed in Fig.5.12. This data was recorded at a little over 1.5m above the sea floor. The range of the sonar was less than expected with the response dropping to a negligible level at only 7m from the sonar. Examining the waterfall image it is not possible to detect a target response that would benefit from

synthetic aperture processing. There does not appear to be any responses that can be correlated between pings.

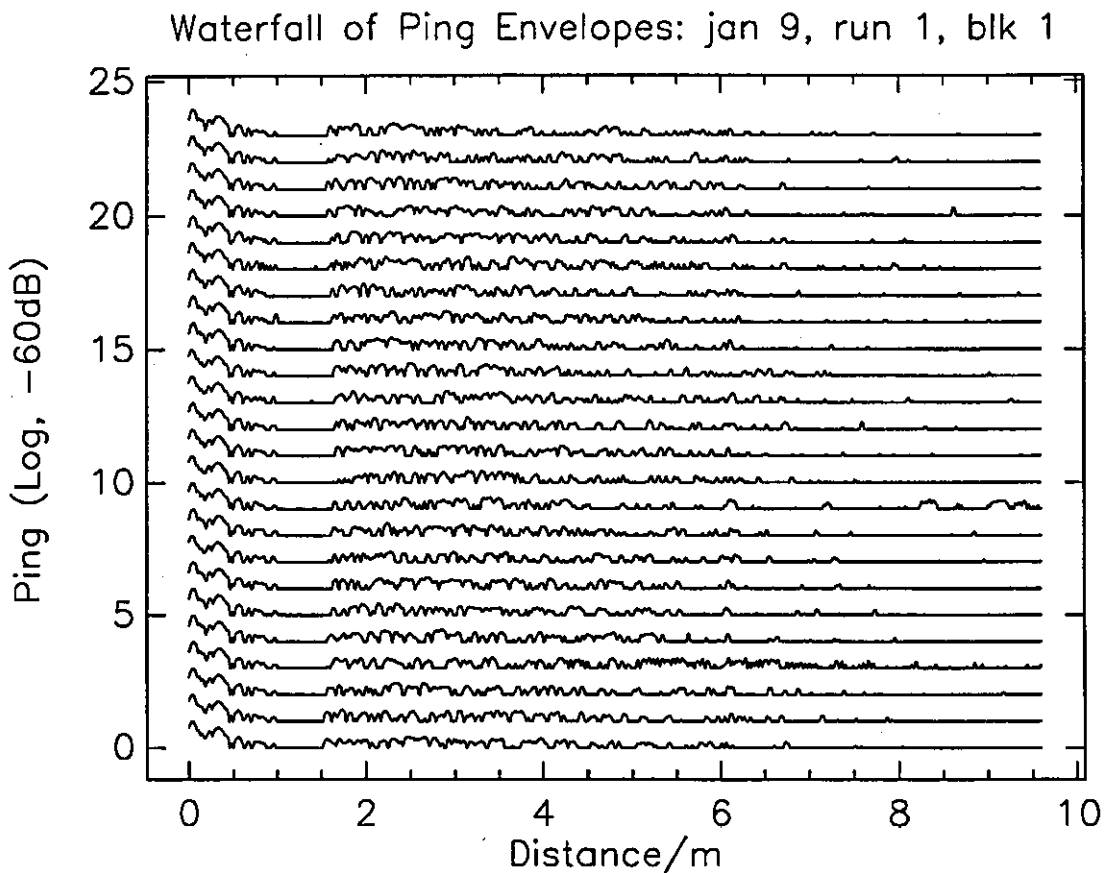


**Fig.5.12** Waterfall Image of Receive Amplitude

A second waterfall image from a different location is displayed in Fig.5.13. At this location the towbody is higher above the sea floor. Again it is not possible to detect a target response that is correlated between pings.

#### 5.4.4 Conclusions From Field Experiments

It is unfortunate that no definitive conclusions can be made from the experiments that were to be the culmination of this work. The data corruption that occurred from the degradation of the underwater electronics package destroyed the data from most of the acoustic sensors. From the data that was available it was not possible to readily identify responses that would have benefited from synthetic aperture processing.

Waterfall of Ping Envelopes: jan 9, run 10, blk 3

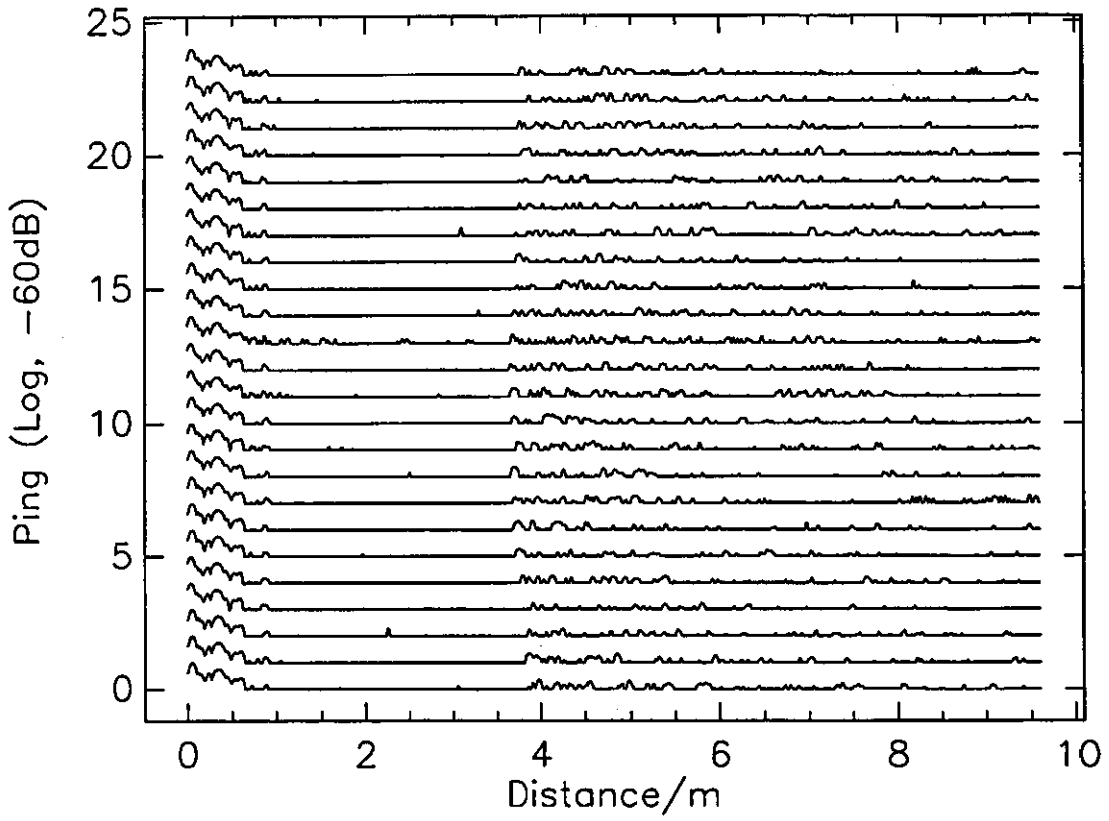


**Fig.5.13** Waterfall Response of a Single Element

## Chapter 6 Conclusions

### 6.1 Discussion

The goal of producing a synthetic aperture sonar has been realised in this thesis. The three novel areas of motion measurement, broadband operation and multiple receivers have been successfully incorporated in the design. Considerable effort was invested in producing this system across a diverse range of disciplines. Further effort was involved in trialing the system and processing the large sets of data afterwards.

The motion measuring equipment used in the sonar successfully measured motions of the underwater platform when towed behind a surface vessel. These measurements were not intended to have sufficient accuracy to measure the trajectory of the sonar to produce motion compensated synthetic aperture images directly. The sensors were not sufficiently sensitive for sub-wavelength motion reckoning at the operational frequency. The processed data did demonstrate the inability of the sensors to accurately determine low frequency motion. The sensors were more successful at measuring higher frequency motion.

The motion measurements demonstrated the desirability of a stable towfish for synthetic aperture imaging. They also showed the large motions that are experienced in shallow water where little cable is available for damping the effect of tow vessel motion on the sonar.

The acoustic sensors were found to operate as expected over the frequency range of the sonar. The underwater and surface electronics worked well in recording the acoustic data when deployed in the test tank. However, the electronics interfacing to the sensors had deficiencies that effected the field trials particularly. The analogue gain sections required a greater dynamic range for better range performance. The most severe deficiency became progressively worse through the duration of the trials and involved an inexplicable degradation of the pins of the electronic devices in the atmosphere of the underwater canister. The result of this was an uncorrectable

corruption of digitised values of the sensor waveforms. This ultimately restricted the image formation processing that could be performed with the data.

The test tank measurements were a mixed success. An assumption made for the data processing was that the array was steady in the tank when the data was collected. However, after processing it became apparent that this premise was not necessarily so. Instead of the image sharpening as the synthetic aperture was increased in length it was degraded with the targets being smeared.

The processing of the field trial data was limited by the data corruption from the degradation of the underwater electronics. Only one transducer was available instead of the planned six. With only one sensor operational the aperture was considerably undersampled. As such only waterfall plots were presented as it is possible to observe targets in the waterfall that would benefit from aperture synthesis. A further limitation with this data was the restricted range.

Many of the deficiencies of the acoustic electronics could have been rectified had more time been available for the trials. The entire sonar system was rather ambitious and would have benefited from further testing in the ocean environment. This testing would have exposed the potential flaws so that corrective actions could have been taken in advance of the final experiments.

## **6.1 Further Investigation**

The combination of measured motion with a good acoustic data set would allow the investigation of the image improvement algorithms. It is likely that such measured motion would improve the likelihood of a synthetic aperture sonar becoming available for wider commercial use.

The use of multiple receive sensors for improving tow speed still remains to be experimentally investigated. Although the theory of such is encouraging, the practice of implementing a system is sure to raise complications with the application.

## References

- Adams, A. E., Lawlor, M. A., Riyait, V. S., Hinton, O. R. and Sharif, B. S. (1996)  
"Real-time Synthetic Aperture Sonar Processing System,"  
IEE Proc. Radar, Sonar Navig., Vol. 143, No. 3, June, pp. 169-176.
- Blacknell, D. and Quegan, S. (1991) "SAR Motion Compensation Using Autofocus,"  
Int. J. Remote Sensing, Vol. 12, No. 2, pp. 253-275.
- Bruce, M. P. (1992) "A Processing Requirement and Resolution Capability  
Comparison of Side-Scan and Synthetic-Aperture Sonars,"  
IEEE J. Ocean. Eng., Vol. 17, No. 1, Jan., pp. 106-117.
- Bucknam, J. N., Chwastyk, A. M., Black, H. D. and Paddison, F. C. (1971)  
"Synthetic Aperture Sonar,"  
Tech. Memo TG1161A, Applied Physics Lab, John Hopkins Uni.
- Chatillon, J., Bouhier, M. and Zakharia, M. E. (1992) "Synthetic Aperture Sonar for  
Seabed Imaging: Relative Merits of Narrow-Band and Wide-Band  
Approaches,"  
IEEE J. Ocean. Eng., Vol. 17, No. 1, Jan., pp. 95-105.
- Checketts, D. G., Smith, B. V. (1986) "Analysis of the Effects of Platform Motion  
upon Various Sonar,"  
Proc. I.O.A., Vol. 8, pp. 135-143.
- Christoff, J. T., Loggins, C. D. and Pipkin, E. L. (1982) "Measurement of the  
Temporal Phase Stability of the Medium,"  
J. Acoust. Soc. Am., Vol. 71, No. 6, Jun., pp 1606-1607.
- Cutrona, L. J. and Hall, G. O. (1962)  
"A Comparison of Techniques for Achieving Fine Azimuth Resolution,"  
IRE Trans. Mil. Elec., MIL-6, April, pp. 119-121.
- Cutrona, L. J., Vivian, W. E., Leith, E. N. and Hall, G. O. (1961)  
"A High-Resolution Radar Combat-Surveillance System,"  
IRE Trans. Mil. Elec., MIL-5, April, pp. 127-131.
- Cutrona, L. J., (1975) "Comparison of Sonar System Performance Achievable Using  
Synthetic Aperture Techniques with the Performance Achievable by More  
Conventional Means,"  
J. Acoust. Soc. Am., Vol. 58, No. 2, Aug., pp 336-348.



- Cutrona, L. J., (1977) "Additional Characteristics of Synthetic Aperture Sonar Systems and a Further Comparison with Non-synthetic Aperture Sonar Systems,"  
J. Acoust. Soc. Am., Vol. 61, No. 5, May, pp 1213-1217.
- Douglas, B. L., Lee, H. (1992) "Synthetic Aperature Active Sonar Imaging,"  
Proc. ICASSP 92, Vol. 3, pp. 37-40
- Douglas, B. L., Lee, H. (1993) "Synthetic Aperature Sonar Imaging with a Multiple Element Receiver Array,"  
Proc. ICASSP 93, Vol. 5, pp. 445-448
- Fox, P. (1985) "An Electronically Focussed Multiple Beam Side Scan Sonar,"  
PhD. Dissertation, University of Cape Town, South Africa.
- Ghiglia, D. C., Mastin G. A. (1989) "Two-dimensional Phase Correction of Synthetic Aperture Radar Imagery,"  
Optics Lett. Vol. 14, No. 20, Oct., pp. 1104-1106.
- Gough, P. T., Hayes, M. P. (1989) "Test Results Using a Prototype Synthetic Aperture Sonar,"  
J. Acoust. Soc. Am., Vol. 86, No. 6, Dec., pp. 2328-2333.
- Gough, P. T., Hayes, M. P. (1989) "Measurement of Acoustic Phase Stability in Loch Linnhe, Scotland,"  
J. Acoust. Soc. Am., Vol. 86, No. 2, Feb., pp. .
- Hayes, M. P., Gough, P. T. (1992) "Broad-Band Synthetic Aperture Sonar,"  
IEEE J. Ocean. Eng., Vol. 17, No. 1, Jan., pp. 80-94.
- deHeering, P. (1984) "Alternate Schemes in Synthetic Aperture Sonar Processing,"  
IEEE J. Ocean. Eng., Vol. OE-9, No. 4, Oct., pp 277-280.
- Heimiller, R. C. (1962) "Theory and Evaluation of Gain Patterns of Synthetic Arrays,"  
IRE Trans. Mil. Elec., MIL-6, April, pp. 111-115.
- Huxtable, B. D. and Geyer, E. M. (1993) "Motion Compensation Feasibility for High Resolution Synthetic Aperture Sonar,"  
IEEE J. Ocean. Eng,
- Ikeda, O., Sato, T. and Suzuki, K., (1979a) "Super-resolution Imaging System Using Waves with a Limited Frequency Bandwidth, "  
J. Acoust. Soc. Am., Vol. 65, No. 1, Jan., pp. 75-81.

- Ikeda, O., Sato, T. and Ohshima, H., (1979b) "Synthetic Apertures Sonar in Turbulent Media, "  
 J. Acoust. Soc. Am., Vol. 66, No. 1, Jul., pp. 209-218.
- Ikeda, O., Sato, T., (1980) "Further Examination of Synthetic Aperture Sonar in Turbulent Medium, "  
 J. Acoust. Soc. Am., Vol. 68, No. 2, Aug., pp. 516-522.
- Ikeda, O., Sato, T. Minamide, Y. and Fukushima, A., (1985) "Image Reconstruction from Disturbed Synthetic Aperture Sonar Data with Aperture Division, "  
 J. Acoust. Soc. Am., Vol. 78, No. 1, July, pp. 112-119
- Johnson, K. A., Hayes, M. P. and Gough, P. T., (1995) "A Method of Estimating the Sub-wavelength Sway of a Sonar Towfish,"  
 IEEE J. Ocean Eng., Vol. 20, No. 4, October, pp. 258-267.
- Kirk, J. C., (1975) "Motion Compensation for Synthetic Aperture Radar,"  
 IEEE Trans. Aero. and Elect. Sys., Vol. AES-11, No. 3, May, pp. 338-348.
- Kock, W. E., (1972) "Extending the Maximum Range of Synthetic Aperture (Hologram) Systems,"  
 Proc. IEEE, Vol. 60, No. 1, Nov, pp. 1459-1460.
- Laughton, A. S. (1981) "The First Decade of GLORIA,"  
 J. Geoph. Res., 86 (B12), pp. 11511-11534.
- Lee, H. E. (1979) "Extension of Synthetic Aperture Radar Technique to Undersea Applications,"  
 IEEE J. Ocean. Eng., Vol. OE-4, No. 2, April, pp. 60-63.
- Loggins, C. D., Christoff, J. T. and Pipkin, E. L. (1982) "Results from Rail Synthetic Aperture Experiments,"  
 J. Acoust. Soc. Am. Suppl. 1, Vol. 1, No. 71.
- Meng, Z and Griffiths, J. W. R. (1993) "A 'Real Time' Experimental Synthetic Aperture Sonar and a Study onn Autofocus in Sonar Environment"  
 Proc. I. O. A. Vol. 15, Part 2, pp 181-186.
- Rolt, K. D., Schmidt, H. (1992) "Azimuthal Ambiguities in Synthetic Aperture Sonar and Synthetic Aperture Radar Imagery,"  
 IEEE J. Ocean. Eng., Vol. 17, No: 1, Jan., pp. 73-79.
- Sato, T., Mitsuhiro, U. and Fukuda, S., (1973) "Synthetic Aperture Sonar,"  
 J. Acoust. Soc. Am., Vol. 54, No. 3, Aug., pp 799-802

- Sato, T., Ikeda, O., (1977a) "Sequential Synthetic Aperture Sonar System - a prototype of a synthetic aperture sonar system,"  
IEEE Trans. on Sonics and Ultrasonics, Vol. SU24, No. 4, July, pp 253-259
- Sato, T., Ikeda, O., (1977b) "Super-resolution Ultrasonic Imaging by Combined Spectral and Aperture Synthesis,"  
J. Acoust. Soc. Am., Vol. 62, No. 2, Aug, pp 341-345
- Sherwin, C. W., Ruina, J. P. and Rawcliffe, R. D. (1962)  
"Some Early Developments in Synthetic Aperture Radar Systems,"  
IRE Trans. Mil. Elec., MIL-6, April, pp. 122-129.
- Somers, M. L. and Stubbs, A. R. (1984) "Sidescan Sonar,"  
IEE Proceedings, Vol. 131, Part F, No. 3, June, pp. 243-256
- Wahl, D. E., Eichel, P. H., Ghiglia, D. C. and Jakowatz, C. V. (1994)  
"Phase Gradient Autofocus - a robust tool for high resolution phase correction,"  
IEEE Trans. Aero. and Elect. Sys. Vol. 30, No. 3, July, pp. 827-835.
- Walsh, A. (1967) "Feasibility Study on Synthetic Aperture Array Techniques for High Resolution Ocean Bottom Mapping,"  
Report No. R593, Raytheon Co., Rhode Island, USA, Dec.
- Wiley, C. A. (1965). "Pulsed Doppler Methods and Apparatus,"  
United States Patent, No. 3,196,436.
- Wiley, C. A. (1985). "Synthetic Aperture Radars - A Paradigm for Technology Evolution,"  
IEEE Trans. Aero. Elec. Sys., AES-21, pp. 440-443
- Williams, R. E. (1976) "Creating an Acoustic Synthetic Aperture in the Ocean,"  
J. Acoust. Soc. Am., Vol. 60, No. 1, July, pp 60-73
- Wood, J. W. (1988) "The Removal of Azimuth Distortion in Synthetic Aperture Radar Images,"  
Int. J. Rem. Sensing, Vol. 9, No. 6, pp. 1097-1107.



